FINAL REPORT on

CLEAN CAST STEEL TECHNOLOGY:
EFFECT OF MICRO-POROSITY ON TENSILE AND CHARPY PROPERTIES OF FOUR CAST STEELS

By

JOHN A. GRIFFIN

And

CHARLES E. BATES
UNIVERSITY OF ALABAMA AT BIRMINGAM

TO

THE DEPARTMENT OF ENERGY,

And

THE STEEL FOUNDERS' SOCIETY OF AMERICA

DOE CONTRACT N0. DE-FC36-02ID14229

REPORT NO. 527992-2005 Project Final Report

September 2005

CLEAN CAST STEEL TECHNOLOGY:
EFFECT OF MICRO-POROSITY ON TENSILE AND CHARPY PROPERTIES OF FOUR CAST STEELS

Table of Contents

Clean Cast Steel Technology:
Effect of Micro-porosity on Tensile and Charpy Properties of Four Cast Steels

Executive Summary

The effect of these large shrink cavities on mechanical properties could be easily calculated using well established engineering formulas. Over the years, increases in computational and metallurgical resources have allowed the modeler to improve accuracy and increase the complexity of numerical predictors. An accurate prediction of micro-porosity, not observable using conventional radiographic techniques, and an engineering understanding of the effect on mechanical properties would give a designer confidence in using a more efficient casting design and a lower safety factor. This will give castings an additional design advantage. The goal of this project is to provide current and future modelers/designers with a tensile and Charpy property dataset for validation of micro-porosity predictors.

The response of ultimate strength, elongation, and reduction in area to micro-porosity was very similar in all four alloys. Ultimate strength was largely unaffected by tensile fracture surface porosity until values of about 25% were reached and decreased linearly with increasing values. Elongation and reduction in area decreased sharply after less than 5% fracture surface porosity. Niyama values of about 0.7 were produced sound material and acceptable tensile properties. Ultrasonic velocities of 0.233 in/usec and higher produced acceptable tensile properties. Metallographic examination revealed a ratio of 4-6 to 1 in fracture surface porosity to metallographic porosity.

Charpy impact properties were largely unaffected by the microporosity concentrations examined in this study and did not correlate to either Niyama values, fracture surface porosity, or metallographic porosity.

Clean Cast Steel Technology:
Effect of Micro-porosity on Tensile and Charpy Properties of Four Cast Steels

1. INTRODUCTION

A variety of numerical methods for predicting casting porosity has been developed over the past sixty years.[1-6]. Initially, these techniques were used to predict large macro-shrink that could be easily observed with radiography. The effect of these large shrink cavities on mechanical properties could be easily calculated using well established engineering formulas. Over the years, increases in computational and metallurgical resources have allowed the modeler to improve accuracy and increase the complexity of numerical predictors and there is reason to expect that this trend will continue in the future. An accurate prediction of micro-porosity, not observable using conventional radiographic techniques, and an engineering understanding of the effect on mechanical properties would give a designer confidence in using a more efficient casting design and a lower safety factor. This will give castings an additional design advantage. The goal of this project is to provide current and future modelers/designers with a tensile and Charpy property dataset for validation of micro-porosity predictors.

Most radiographic techniques used a 2% resolution limit so we identify micro-porosity as a porosity concentration of 2% or less. Only through net section loss can porosity affect yield strength since no plastic deformation occurs until the specimen passes the yield point. Net section loss from micro-porosity (< 2% porosity) is very small and does not significantly affect yield strength with a typical tensile test. Ultimate strength can be affected by moderate levels of porosity while ductility can be significantly affected by micro-porosity. Uram [7] investigated the effect of micro-porosity on a high strength 4340 cast steel by casting a series of plates, solid cylinders, and step wedges to produce a variety of macrostructures, thermal gradients, and feeding conditions. The amount of porosity was measured using a micro-radiography technique, and it was found that a steep thermal gradient produced sound material and with the highest ductility. Porosity values greater than 0.50% significantly reduced both elongation and reduction of area as illustrated in Figure 1.

Larson, Lloyd, and Herlihy [8] correlated tensile properties to radiographic quality in 8735 cast steel. Plates were cast to produce a variety of radiographic and micro-porosity levels. Again it was found that micro-porosity, as measured by a micro-radiography technique, had a significant effect on ductility and ultimate strength, as illustrated in Figure 2. With the exception of gross shrink cavities, porosity did not have a significant effect on yield strength.

The University of Alabama at Birmingham (UAB) conducted a pathfinder trial on micro-porosity effects on 1025 normalized carbon steel tensile properties. Careful analysis of the data showed an effect of porosity on yield and ultimate strength at high porosity levels (>50% of the fracture surface was shrink porosity). The population for the high porosity specimens had a skewed normal distribution compared to a normal distribution in the low micro-porosity

specimens. The largest effect was in elongation and reduction of area where less than 20% fracture surface porosity reduced elongation and reduction of area by 50%.

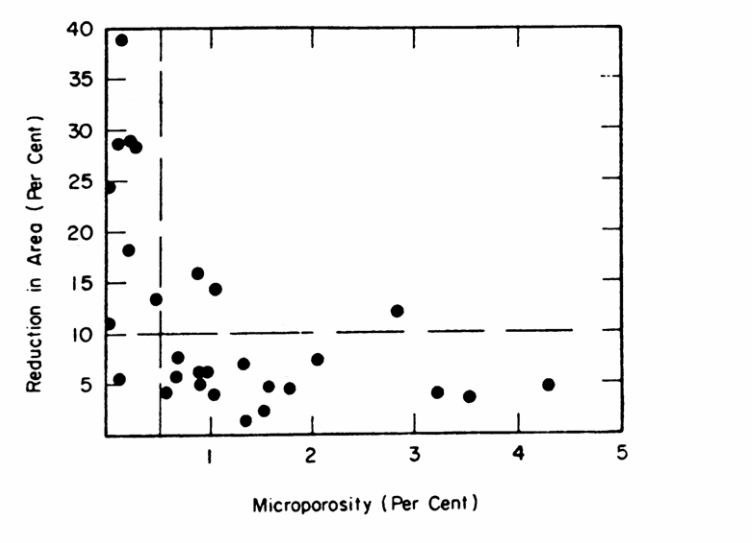

Figure 1. Effect of Micro-Porosity on Reduction of Area (Uram).

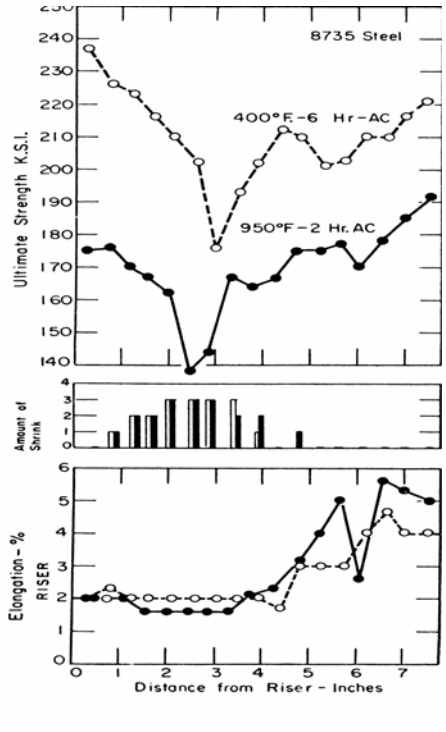

Figure 2. Properties in Cast 8735 Plate - 8 in. Long. Tensile Samples were 0.020 in x 0.875 in. (Larson).

2. PROCEDURES

This paper will report the results of tensile and Charpy properties from an 8630 Q&T (ASTM 958-00 Grade SC 8630 Class 90/60) cast steel, a 4325 Q&T (Class 130/115) cast steel, a CA6 NM (ASTM A487), and a CD3 NM (ASTM A890 Grade 4A). Tensile tests were conducted according to ASTM E8/A370, and the Charpy tests were conducted at a temperature of -40°F and followed ASTM E23/A370. The test plates and blanks removed from the test plates were radiographed and ultrasonically tested.

The 8630 plates were normalized for 2 hours at 1700°F, quenched into 85-95°F water at 1650°F, and tempered for 2 hours at 1200°F. The steel contained 0.29% C, 0.934% Mn, 0.664% Si, 0.5% Ni, 0.49% Cr, 0.27% Mo, 0.045% Al, 0.027% P, and 0.022% S. A schematic of the test plate is illustrated in Figure 4. The plate was approximately 32" long, 6" wide, and 3" thick and fed with a 6" diameter riser.

The 4325 plates were normalized for 12 hours at 1600°F before riser removal, normalized for 10 hours at 1600ºF, tempered for 11 hours 1250ºF, austenitized for 9 hours at 1600ºF, quenched into 80°F water, and tempered for 11 hours at 1115°F. The steel contained 0.30% C, 0.88% Mn, 0.46% Si, 1.79% Ni, 0.85% Cr, 0.44% Mo, 0.015% P, and 0.015% S. A schematic of the test plate is illustrated in Figure 3. The plate was approximately 41" long, 6" wide, and 3" thick and fed with a 6" diameter riser. A five inch long extension and chill were added to the left of the riser to produce very sound metal as a reference.

The CA6NM plates were heat treated according to ASTM A487 Class B (100/75) by austenitizing at 1850ºF , cooling below 200ºF, and intermediate tempering at 1225-1275ºF and a final temper at 1050-1150ºF. A schematic of the test plate design is illustrated in Figure 4. The plate was approximately 32" long, 6" wide, and 3" thick and fed with a 6" diameter riser. The CD3 NM (ASTM A890 Grade 4A plates were heat treated according to ASTM A890 by 2050ºF and water quenching. A schematic of the test plate design is illustrated in Figure 4. The plate was approximately 32" long, 6" wide, and 3" thick and fed with a 6" diameter riser. These plates were designed to produce varying levels of porosity along its length with porosity levels increasing as the distance from the left side of the plate increased.

Each plate was sliced into 1" thick sections and identified for location as illustrated in Figure 5. For the 4325 plates, samples 1 through 6 were to the left of the riser with sample 1 adjacent to the chill and sample 6 only partially underneath the riser. Samples 7 through 12 were located below the riser while samples 13 through 41 were located to the right of the riser with increasing numbers indicating increasing distance from the chilled end of the casting. Plates for the other three alloys were similarly treated except samples 1 through 6 were under the riser and samples 7 through 32 were located to the right of the riser with increasing numbers indicating increasing distance from the risered end of the casting.

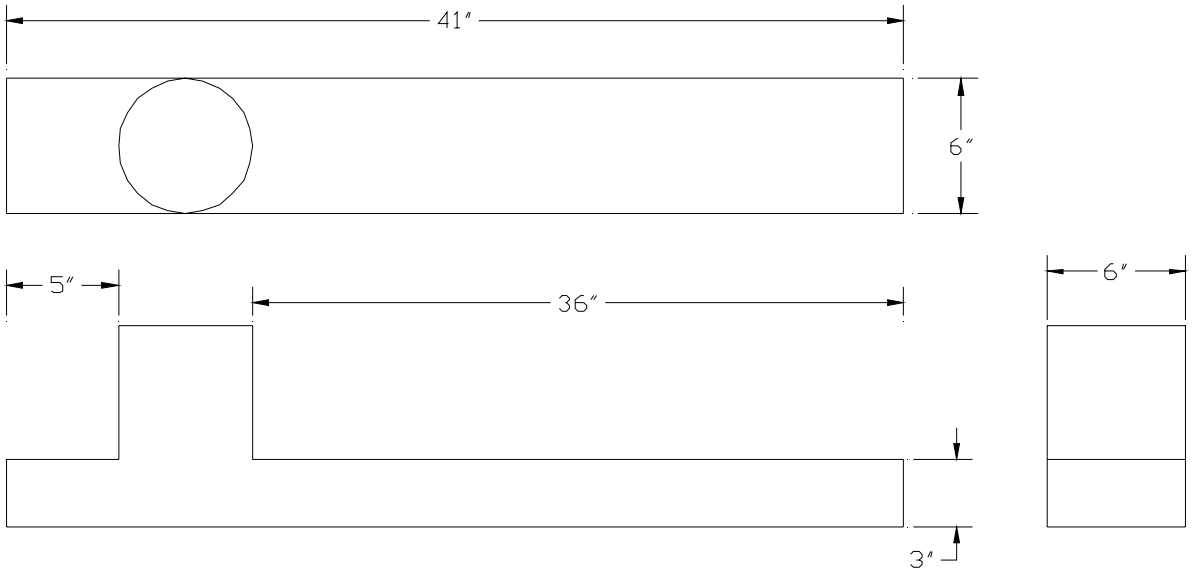

Figure 3. Schematic of Test Plate for alloy 4325 Q&T cast steel.

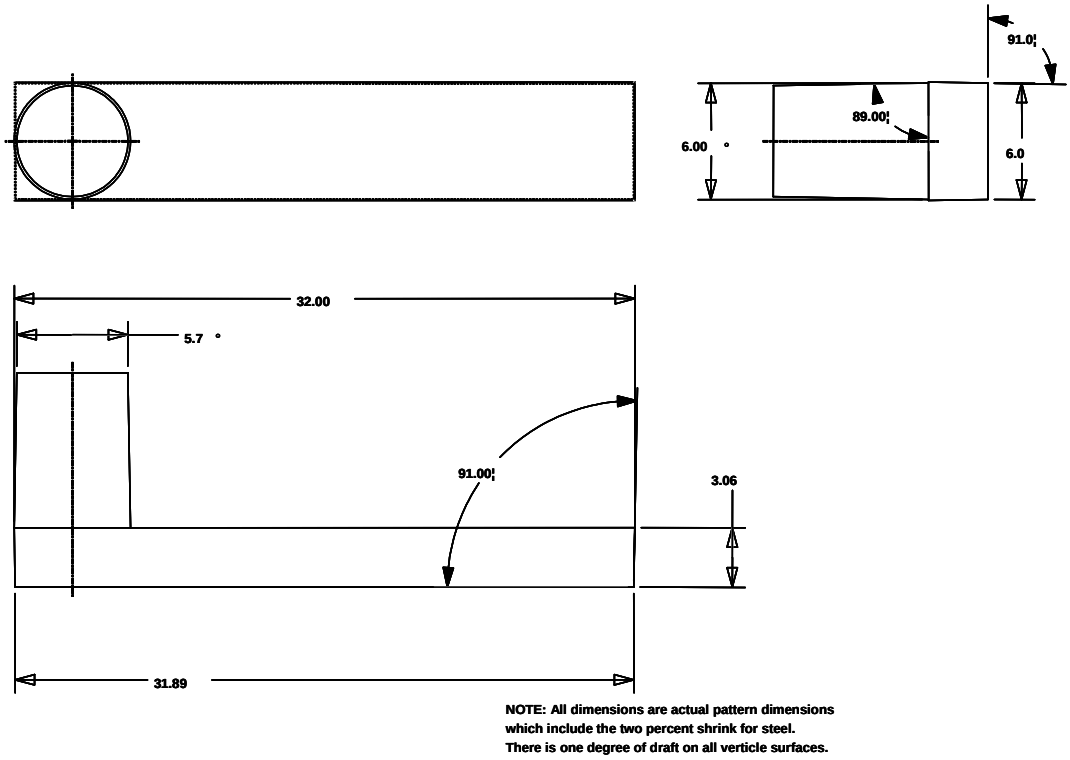

Figure 4. Schematic of Test Plate for alloy 8630 Q&T, CA6NM, and CD3MN.

Tensile and Charpy blanks were removed from the center and drag surface of each section, as illustrated in Figure 6. Tensile and Charpy blanks were removed from sections selected from radiographic examination. The plates, test sections, and specimen blanks were radiographed for examination purposes, as illustrated in Figure 7; however, no comparisons were made at this time since no current radiographic standard exists that relates performance to radiographic rating.

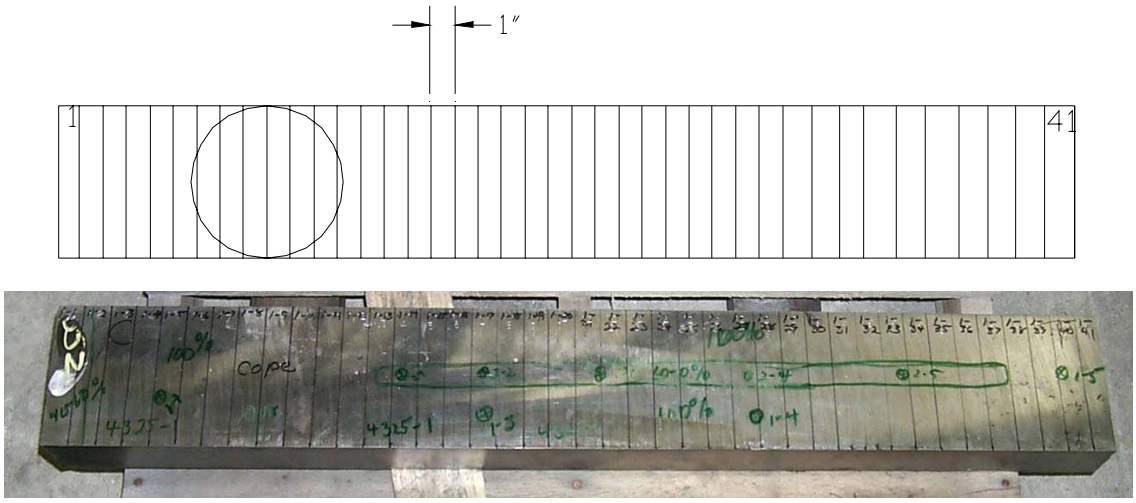

Figure 5 Schematic of Location and Identification of Sections Removed from Test Plate.

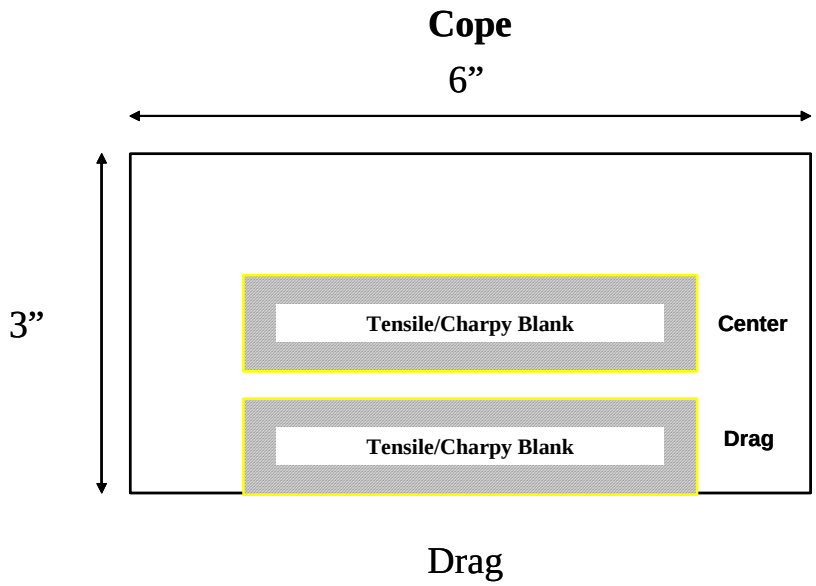

Figure 6. Location and Identification of Specimen Blanks from Each Section Removed from Test Plate.

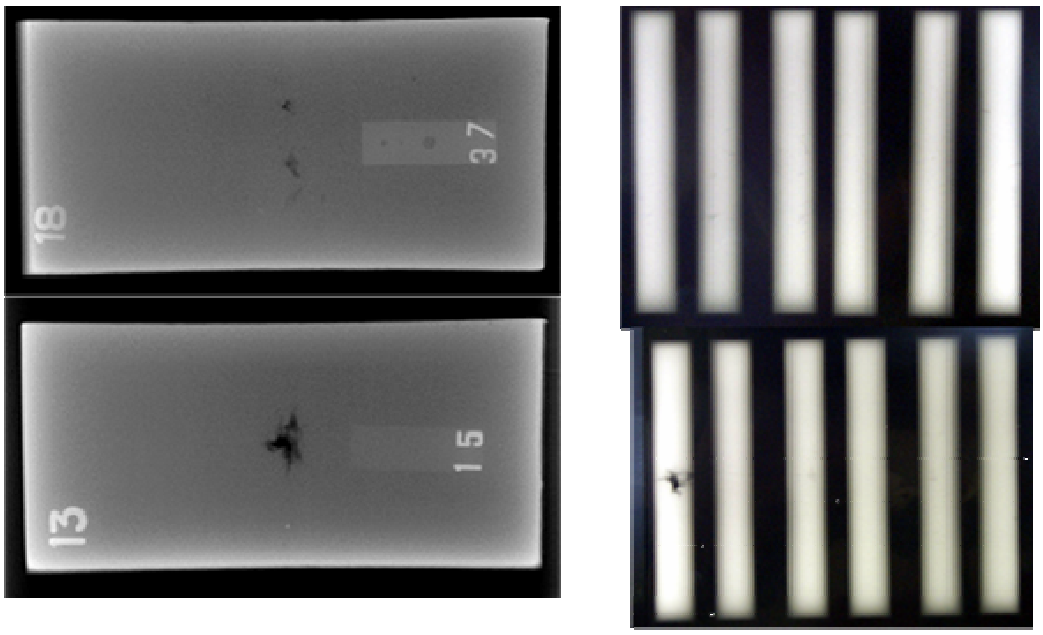

Figure 7. Radiographs of Plate Sections and Specimen Blanks.

The specimen blanks were examined using ultrasonic inspection before final machining. Measurements were made longitudinally as illustrated in Figure 8. This orientation was selected to align the pulse to the tensile stress field. Each blank was scanned through its length and the signals produced by the anomalies were digitally recorded. The transducers were 0.5" in diameter and a straight planar beam design. Frequencies of 2, 5, and 10 megahertz were used.

Figure 8. Ultrasonic measurement location and direction on tensile and Charpy impact specimen blanks.

Ultrasonic inspection was used to measure ultrasonic velocity and signal attenuation (signal loss caused by signal scattering from anomalies) in the thru mode and thru-back modes. Ultrasonic velocity was determined by carefully measuring the time required for the signal to pass through the specimen. An example of the effect of porosity on velocity is illustrated in Figure 9. High concentrations of anomalies typically delay and broaden the ultrasonic wave. For signal attenuation,

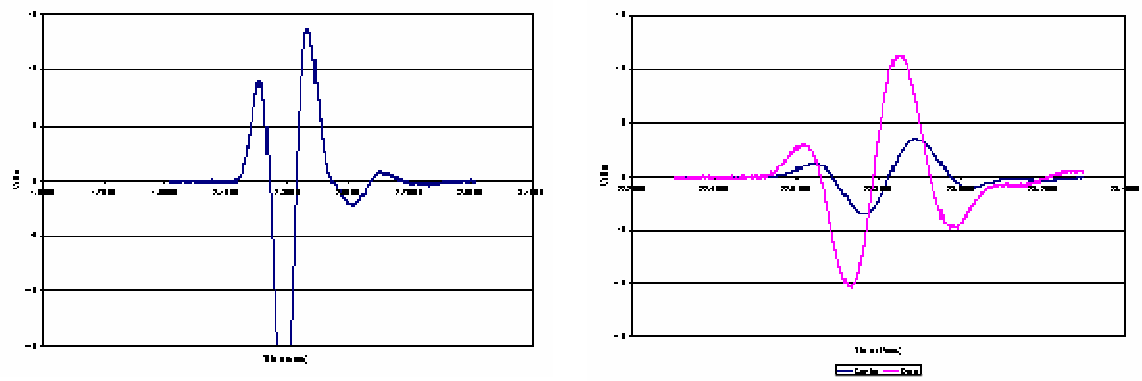

Input Signal **Output Signal**

Figure 9. Example of the Effect of Porosity on Ultrasonic Velocity.

the voltage strength of the main ultrasonic pulse is measured after the pulse has traveled through a known length of material. Total attenuation is calculated using the formula

$$Total\ Attenuation = 20 * \log\left(\frac{V_{Main}}{V_{Backface}}\right).$$

Attenuation is normalized by dividing the total attenuation by path length. The loss in main pulse signal strength is directly proportional to scattering caused by internal anomalies. An example of the effect of porosity on ultrasonic signal strength is given in Figure 10.

After radiographic and ultrasonic inspection, tensile and Charpy specimens were machined from the blanks and tested. A schematic of the tensile and Charpy specimen design are illustrated in Figures 11 and 12. The tensile specimen had a 1.5” gage length with a 0.3” gage diameter. The Charpy specimen design was a standard full-size specimen with a Type A notch. After testing, the fracture surface was examined for any anomalies on the surface. In all cases, porosity was the only anomalous feature observed. Photographs were taken of each fracture surface and percent fraction of the fracture surface area containing porosity was measured by manually tracing the porosity using an image analysis software package.

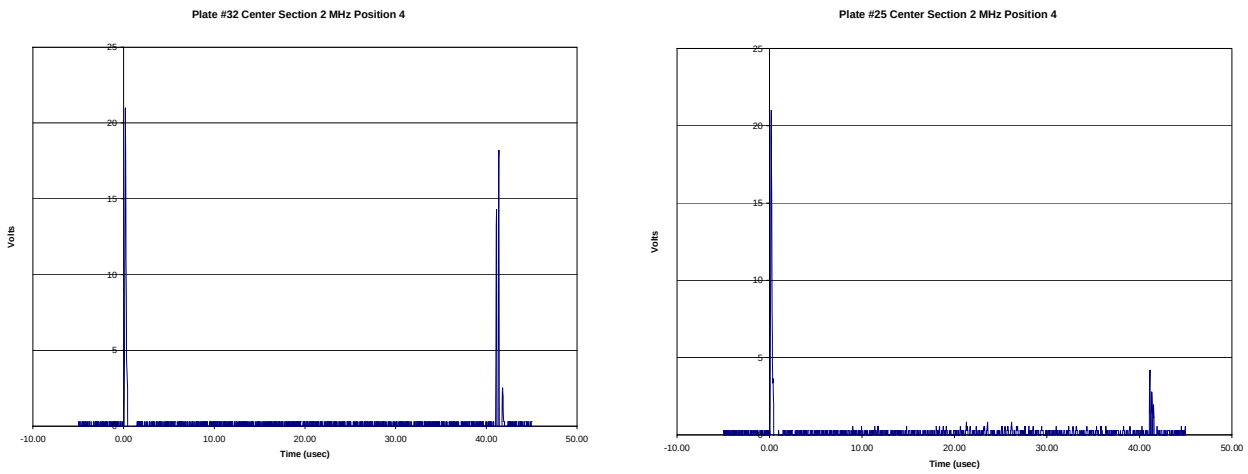

Low Porosity (Drag) **High Porosity (Center)**

Figure 10. Example of the Effect of Porosity on Ultrasonic Signal Strength.

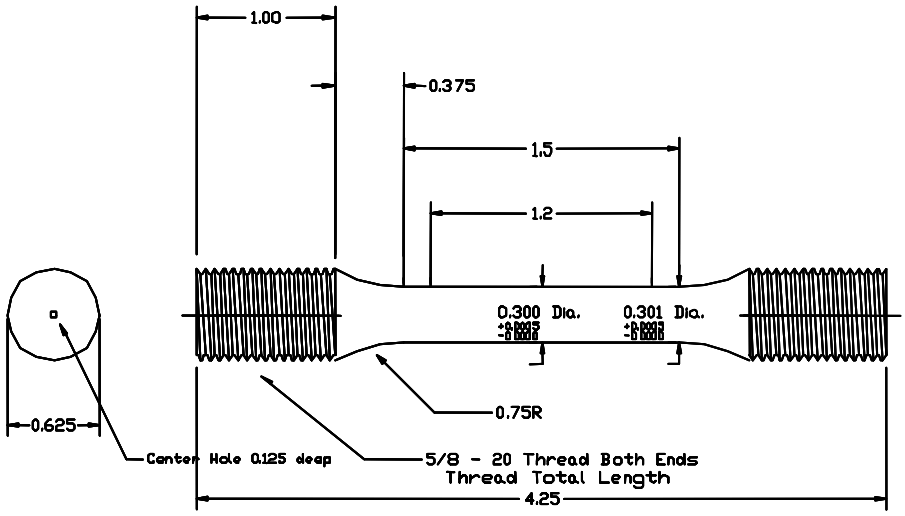

Notes :
1. All Dimensions are in Inches.
2. All Diameters True and Concentric to within +- 0.0005.
3. Do not undercut Radii at Tangent Points.
4. Both Ends to be Flat and Perpendicular to +-0.0005 : Ends need to bottom out in pull rod.
5. Tolerance unless otherwise noted +- 0.001
6. Maximum Thread Load 20,000 lbs. for 12,000 psi thread shear and 150,000 psi UTS.
7. Maximum Load on Pull Rods = 20,000 lbs.

Figure 11. Schematic of Tensile Specimen Design.

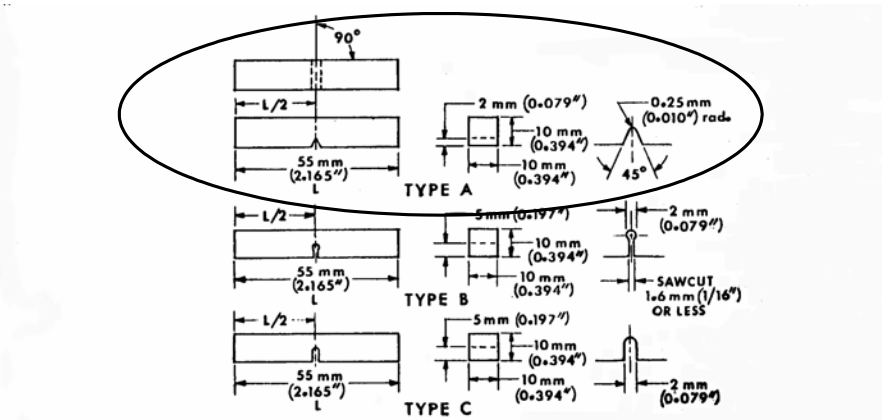

NOTE 1—Permissible variations shall be as follows:

Notch length to edge	90 ±2°
Adjacent sides shall be at	90° ±10 min
Cross-section dimensions	±0.075 mm (±0.003 in.)
Length of specimen (*L*)	+0, −2.5 mm (+0, −0.100 in.)
Centering of notch (*L*/2)	±1 mm (±0.039 in.)
Angle of notch	±1°
Radius of notch	±0.025 mm (±0.001 in.)
Notch depth:	
Type A specimen	±0.025 mm (±0.001 in.)
Types B and C specimen	±0.075 mm (±0.003 in.)
Finish requirements	2 μm (63 μin.) on notched surface and opposite face; 4 μm (125 μin.) on other two surfaces

Figure 12. Schematic of Charpy Impact Specimen Design (Type A).

3. RESULTS AND DISCUSSION

3.1 TENSILE DATA

3.1.1 8630 Quenched and Tempered Cast Steel

A plot of all tensile stress/strain curves to failure for quenched and tempered 8630 is shown in Figure 13. Specimens containing large amounts of porosity can be readily identified by their low strain values before failure. A plot of ultimate tensile strength and 0.2% offset yield strength versus specimen location are illustrated in Figures 14 and 15. Tensile strength is not affected by specimen location near the riser or toe of the test plate. However, away from the high solidification rates associated with the ends of the plate, specimens along the centerline do produce lower tensile properties. This property decrease is not uniform since the shrink porosity is not uniform along the centerline.

Ductility measurements such as elongation and reduction in area are affected to a greater extent by porosity compared to tensile strength. Figure 16 illustrates the relationship between specimen location and elongation in Q&T 8630. The relationship is similar to tensile strength but much exaggerated. The same effect can be seen in the reduction of area data plotted in Figure 17. Fracture surface porosity was measured on each tensile specimen and plotted versus specimen location as shown in Figure 18. The highest fracture surface porosity values appeared

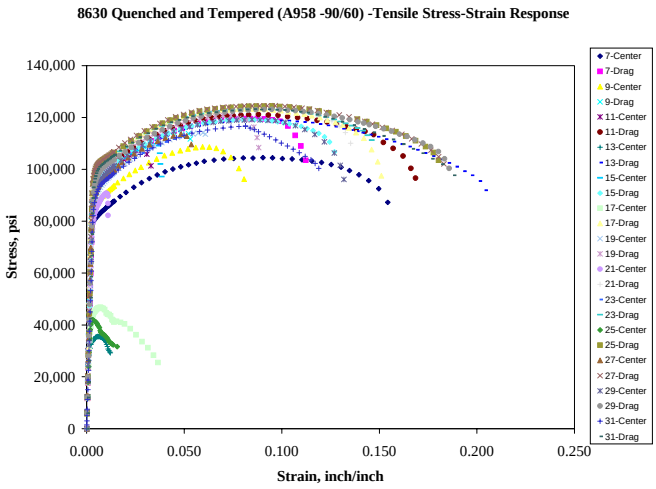

Figure 13. Tensile stress-strain curves for 8630 Q&T cast steel.

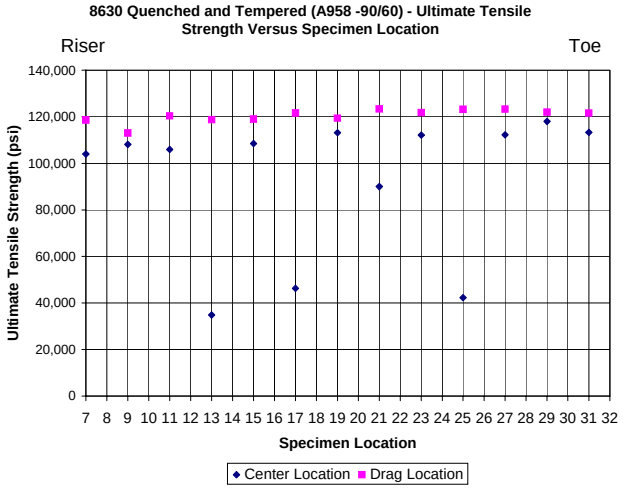

Figure 14. Relationship between ultimate tensile strength and specimen location in 8630Q&T.

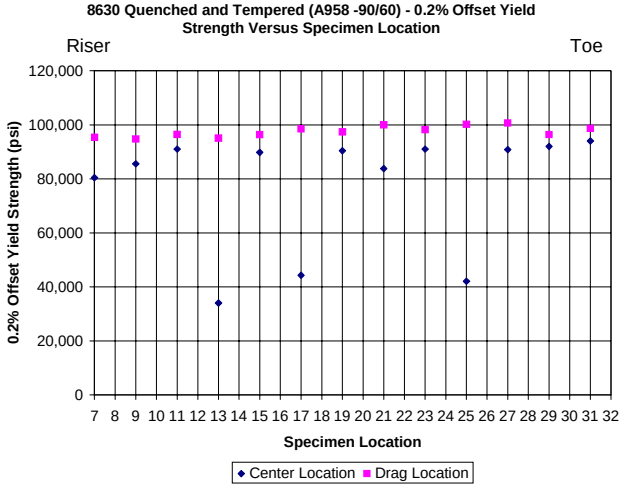

Figure 15. Relationship between yield strength and specimen location in 8630Q&T.

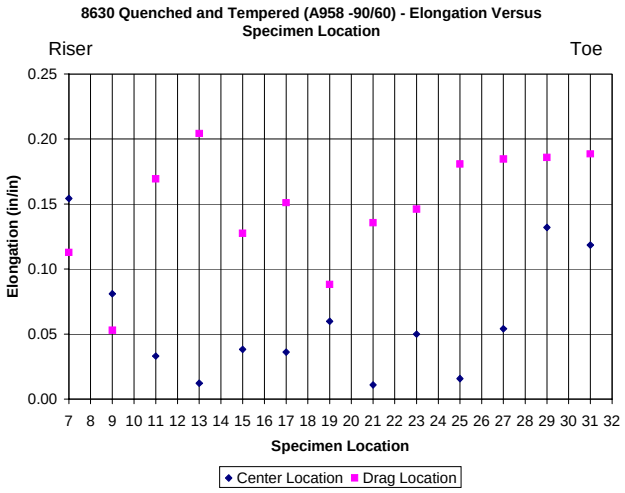

Figure 16. Relationship between elongation and specimen location in 8630Q&T.

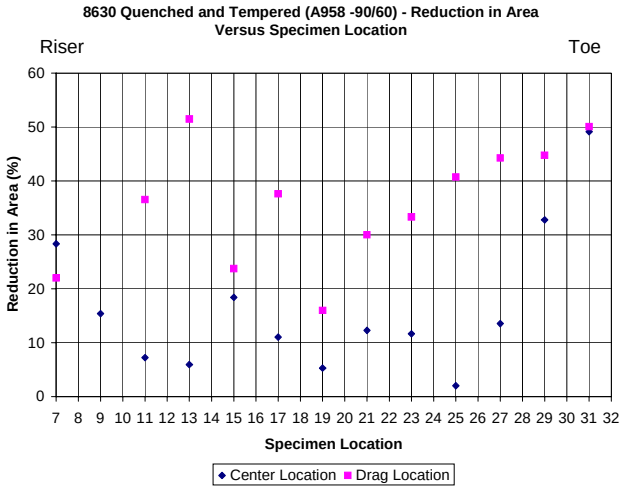

Figure 17. Relationship between reduction in area and specimen location in 8630Q&T.

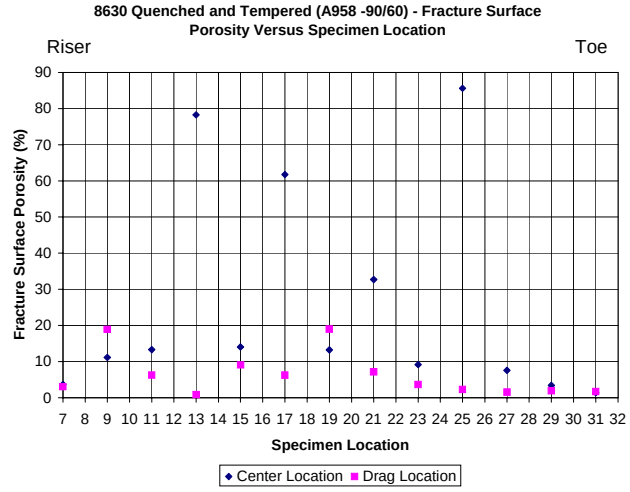

Figure 18. Relationship between fracture surface porosity and specimen location in 8630Q&T.

in specimens located away from the casting riser or toe and near the centerline, as would be expected.

Niyama values were calculated for this simple shape and plotted against tensile strength, elongation and reduction in area, as illustrated in Figures 19, 20, and 21, respectively. A Niyama value of about 0.7 would provide a sufficient thermal gradient to produce low micro-porosity and typical tensile properties for this steel. A similar set of plots for fracture surface porosity are illustrated in Figures 22, 23, and 24. Tensile strength is not affected until fracture surface porosity covers about 30% of the fracture surface. However, as can be seen in Figures 23 and 24, less than 5% fracture surface porosity can sharply reduce elongation and reduction in area.

The sample blanks were ultrasonically tested before machining into tensile specimens. The samples were tested at 2, 5, and 10 MHz which is the frequency range typically used to examine cast steels. The lower frequencies typically are less noisy but are also less likely to interact with smaller sized anomalies such as shrinkage. Conversely, the higher frequencies will detect smaller concentrations of shrink and also unimportant features in the microstructure. Ultrasonic measurements such as velocity or attenuation are an average of the entire bar and do not specifically identify if the anomaly is in the gage section of a tensile specimen. Figures 25 and 26 illustrate the relationship between ultrasonic velocity at 2 MHz and tensile strength and elongation, respectively. Both yield and ultimate strength were unaffected at velocities of about 0.233 in/usec and higher. Elongation required a slightly higher velocity of about 0.2332 in/usec to provide unaffected values.

Attenuation on the tensile specimens was also measured in the through transmission mode. Figure 27 illustrates a plot of attenuation at 2 MHz versus ultimate and yield tensile strength. When attenuation increased from about 0.5 to 1.5 dB/in., both ultimate and yield strength decreased but not significantly. As attenuation continues to increase from 1.5 to 3 dB/in., tensile strength drops rapidly from about 100 ksi to around 40 ksi. Figure 28 illustrates a similar plot of attenuation at 5 MHz versus tensile strength. As a rule, as frequency increases, material attenuation also increases. The 5 MHz attenuation is slightly more sensitive to tensile strength with a steeper decrease in strength as attenuation increases from 1 to 3 dB/in. compared to the 2 MHz data. Attenuation values higher than 3 dB/in. results in a sharp decline in tensile properties.

Figures 29 and 30 illustrate the relationship between ultrasonic velocity at 5 MHz and tensile strength and elongation, respectively. Similar to the 2 MHz data, both yield and ultimate strength were unaffected at velocities of about 0.233 in/usec and higher. Elongation required a slightly higher velocity of about 0.2332 in/usec to provide unaffected values.

A common method for ultrasonically inspecting steel is to measure the strength of the ultrasonic wave reflection from the backface of the part. This is a measurement of attenuation but only requires access to one side of a casting and a reference standard in which to compare the results. The relationship between backface reflection peak height at 2, 5, and 10 MHz and tensile

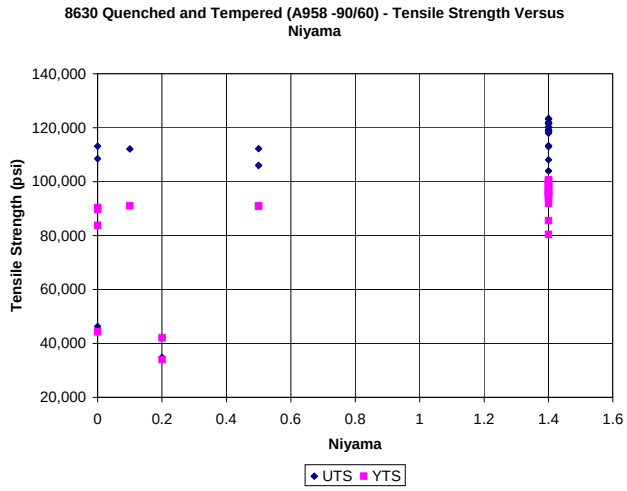

Figure 19. Relationship between tensile strength and Niyama in 8630Q&T.

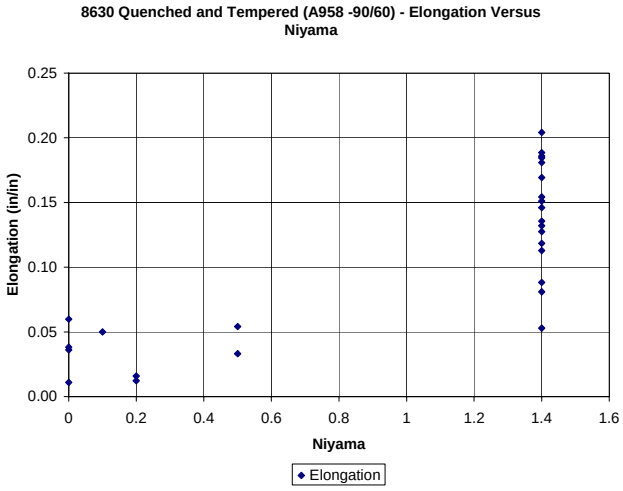

Figure 20. Relationship between elongation and Niyama in 8630Q&T.

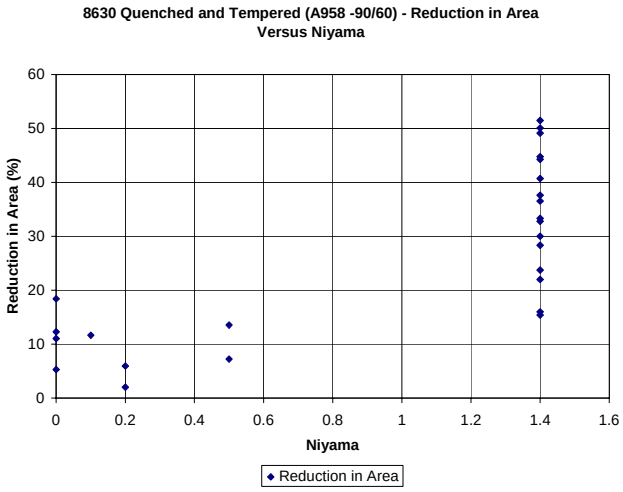

Figure 21. Relationship between reduction in area and Niyama in 8630Q&T.

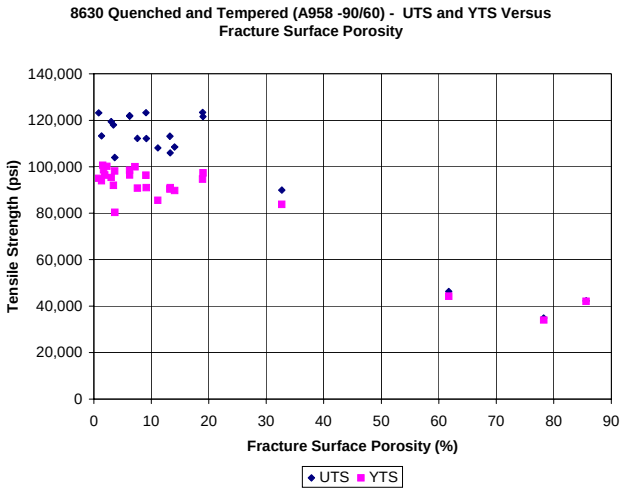

Figure 22. Relationship between tensile strength and fracture surface porosity in 8630Q&T.

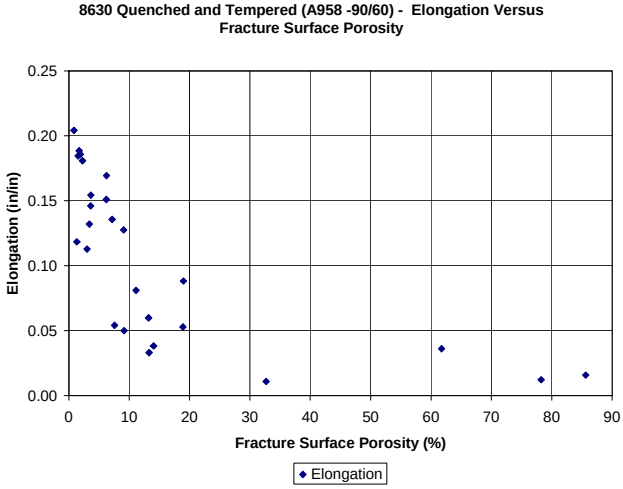

Figure 23. Relationship between elongation and fracture surface porosity in 8630Q&T.

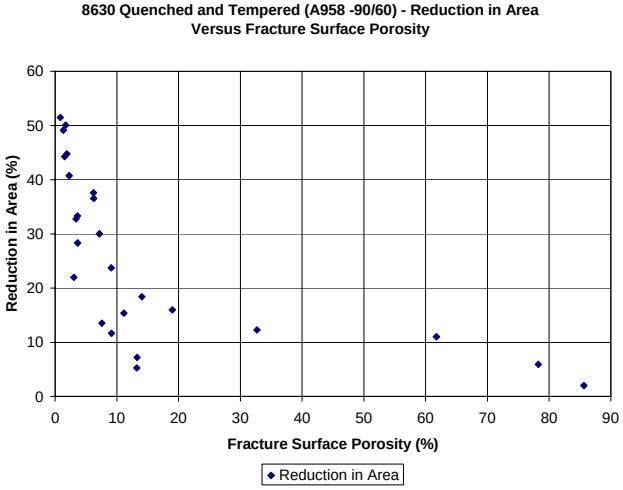

Figure 24. Relationship between reduction in area and fracture surface porosity in 8630Q&T.

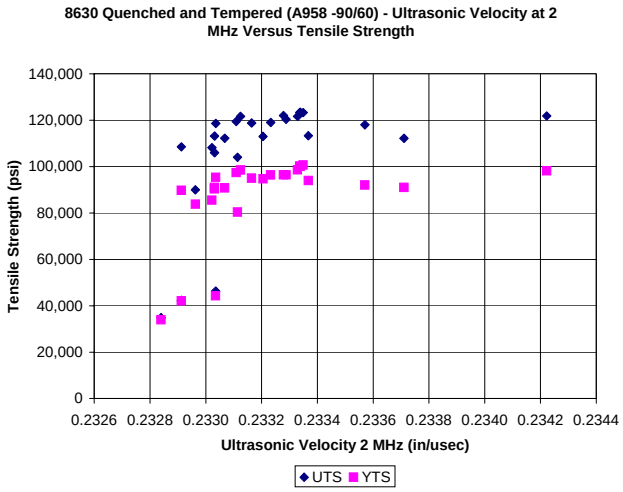

Figure 25. Relationship between tensile strength and ultrasonic velocity in 8630Q&T (2 MHz).

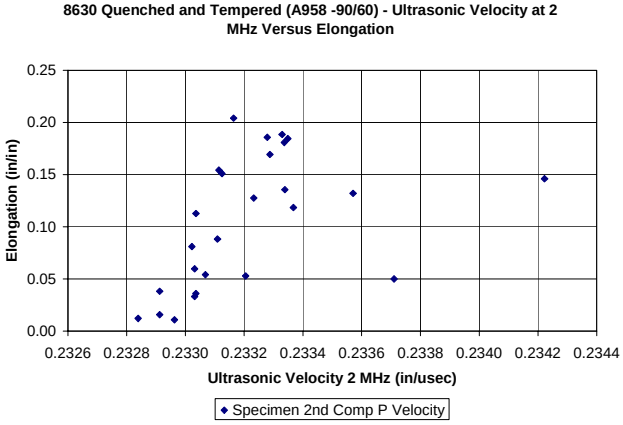

Figure 26. Relationship between elongation and ultrasonic velocity in 8630Q&T (2 MHz).

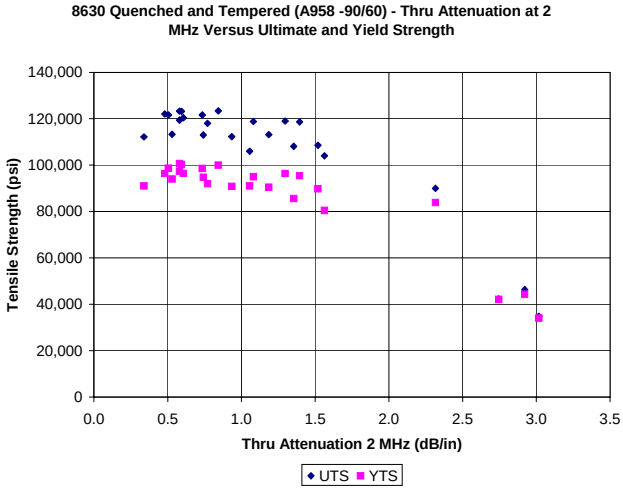

Figure 27. Relationship between tensile strength and ultrasonic attenuation in 8630Q&T (2 MHz).

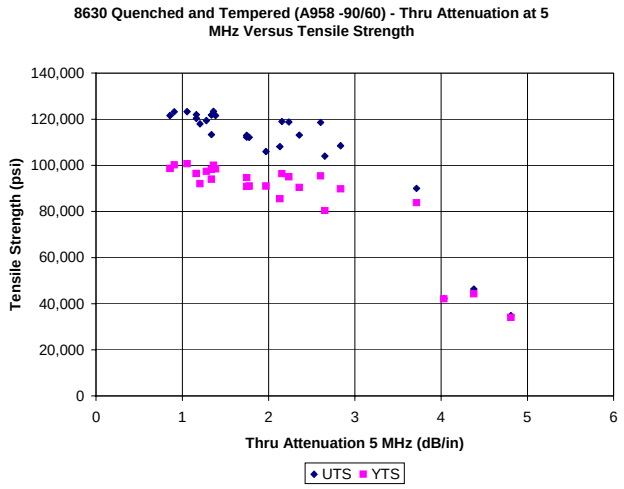

Figure 28. Relationship between tensile strength and ultrasonic attenuation in 8630Q&T (5 MHz).

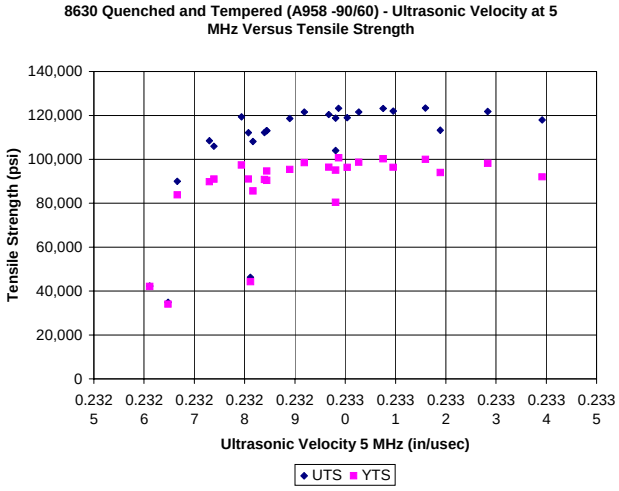

Figure 29. Relationship between tensile strength and ultrasonic velocity in 8630Q&T (5 MHz).

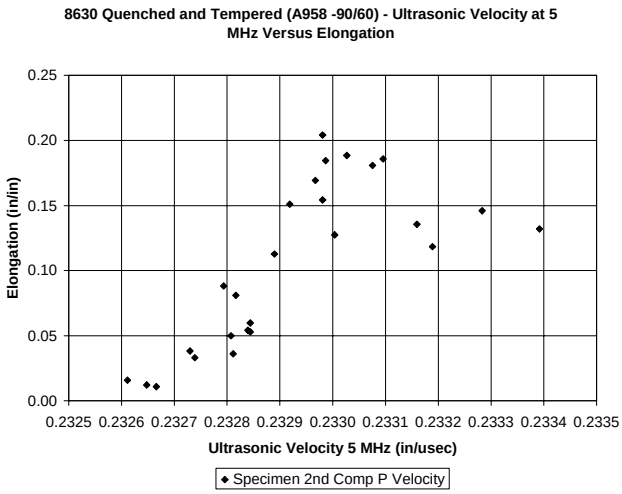

Figure 30. Relationship between elongation and ultrasonic velocity in 8630Q&T (5 MHz).

strength is illustrated in Figures 31 through 33, respectively. At 2 MHz, both ultimate and yield strength slightly decrease as the reflected signal strength decreases from 100 to 60%. A loss of signal strength greater than 50% shows a more rapid decline in tensile properties. At higher frequencies, tensile properties decrease almost linearly from about 100 ksi at 100% reflection strength to about 40 ksi at 20% reflection strength.

A series of graphs showing the correlation between elongation and backface signal strength at 2, 5, and 10 MHz is illustrated in Figures 34 through 36, respectively. The 2 MHz frequency provided the best combination of response and sensitivity. Elongation decreased linearly from 20 to 5% as the backface signal strength decreased from 100 to 60%. The higher frequencies were insensitive to provide an adequate response at these porosity concentrations.

3.1.2 4325 Quenched and Tempered Cast Steel

A plot of all tensile stress/strain curves to failure is shown in Figure 37. Specimens containing large amounts of porosity can be readily identified by their low strain values. Tensile strengths ranged from 90,000 psi up to 167,500 while yield strengths ranged from 139,750 to 155,500 psi. The largest variation was seen in the reduction of area which ranged from 2.7 up to 47.7%. Elongation values ranged from a low of 0.7% up to 18%. The lowest tensile properties were measured in the specimens removed from the center section, as would be expected since that is the most likely location for shrinkage to form.

In Figure 38, the ultimate tensile strength versus specimen location in the casting is illustrated. In the drag samples, there was little variation in the tensile strength along the length of the bar. Values ranged from 158,500 up to 167,500 psi. In the center specimens, the ultimate strength began to drop below 160,000 psi at position 14, which was located a few inches from the right side of the riser. The ultimate strength continued to decrease as the distance from the riser was increased with the lowest value obtained in the sample farthest from the riser. This sample (position 36) had an ultimate tensile strength of only 90,000 psi and this sample fractured out of the gage of the tensile sample.

The yield strength versus sample location is illustrated in Figure 39. The range in yield strength from the drag was narrow as compared to the ultimate strength and only ranged from 151,750 up to 155,750 psi. There was more scatter in the samples from the center although there did not appear to be any relationship between yield and sample location. The yield in the center samples ranged from 139,750 up to 154,750 psi.

Plots for elongation and reduction of area versus specimen location are illustrated in Figures 40 and 41, respectively. Both the center and drag samples showed a drop in ductility and reduction in area as the distance from the riser increased. The drop in elongation and reduction in area was greater in the center samples than in the drag samples and this is probably due to higher porosity content in these samples. The percent elongation was about 16% near the riser and 0.7% at position 16 in the center samples while it ranged from 16 to 8% in the drag samples.

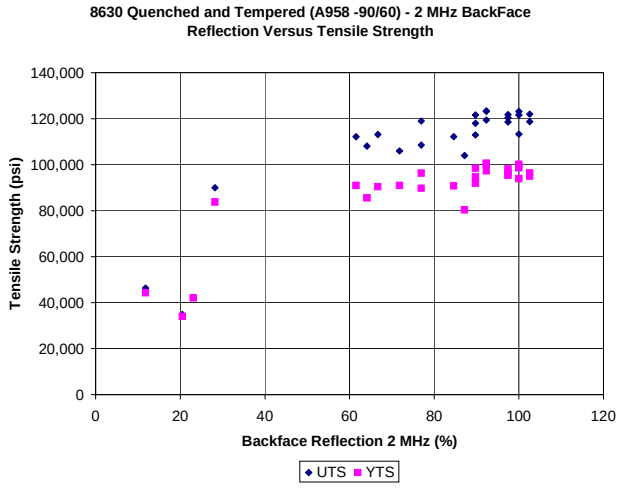

Figure 31. Relationship between tensile strength and ultrasonic backface in 8630Q&T (2 MHz).

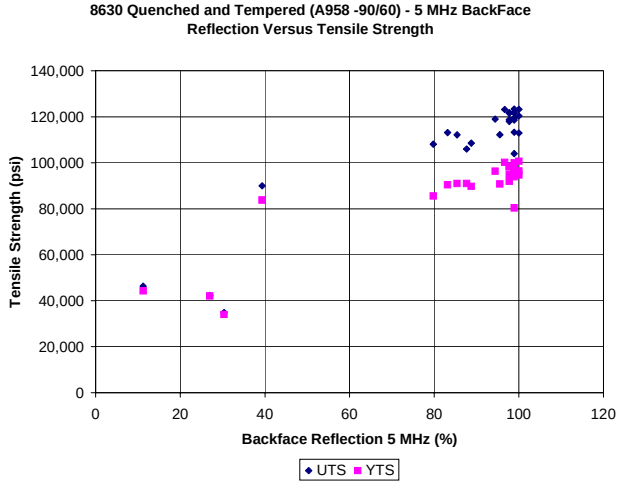

Figure 32. Relationship between tensile strength and ultrasonic backface in 8630Q&T (5 MHz).

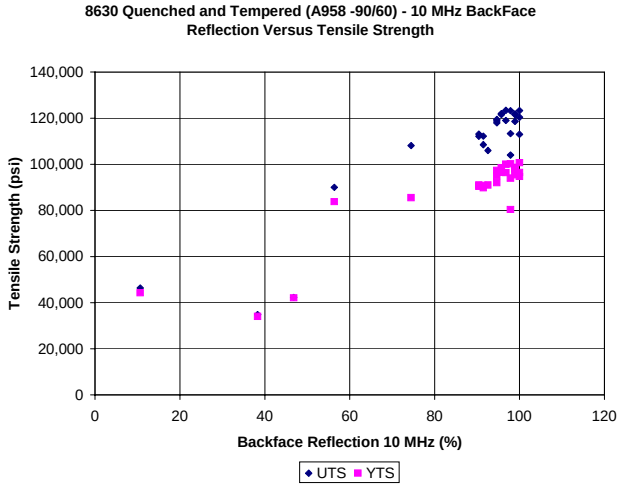

Figure 33. Relationship between tensile strength and ultrasonic backface in 8630Q&T (10 MHz).

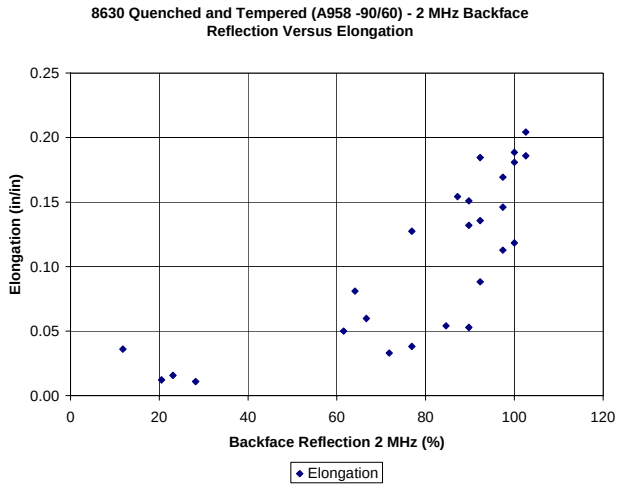

Figure 34. Relationship between elongation and ultrasonic backface in 8630Q&T (2 MHz).

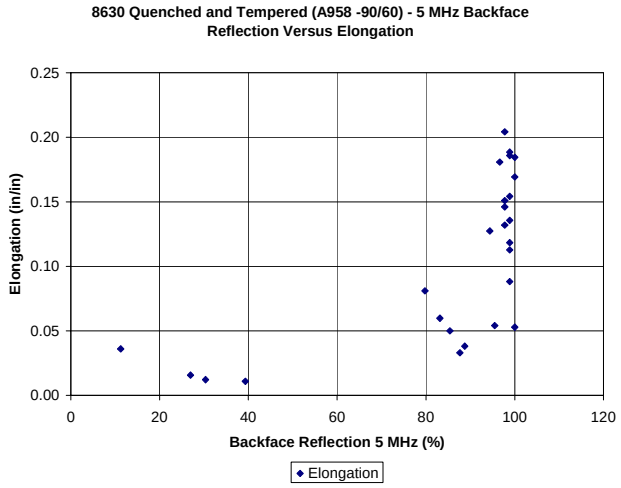

Figure 35. Relationship between elongation and ultrasonic backface in 8630Q&T (5 MHz).

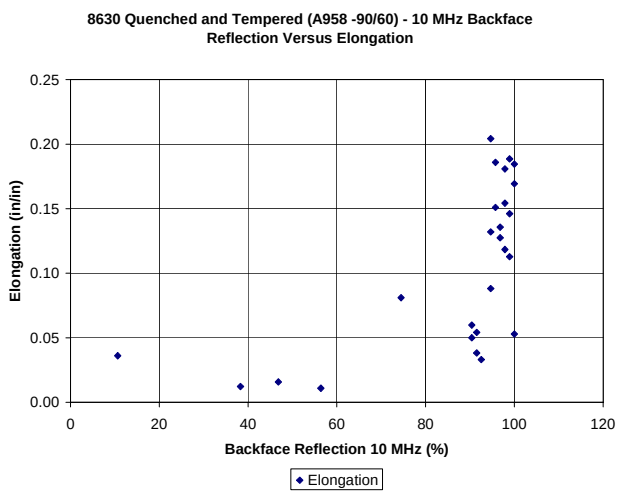

Figure 36. Relationship between elongation and ultrasonic backface in 8630Q&T (10 MHz).

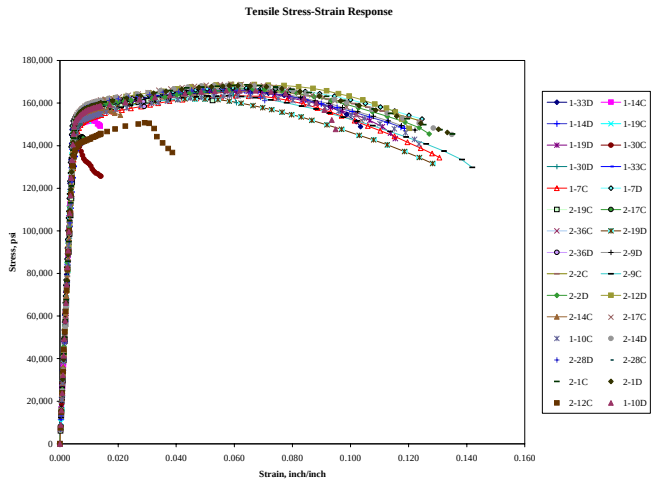

Figure 37. Tensile stress-strain curves for 4325 Q&T cast steel.

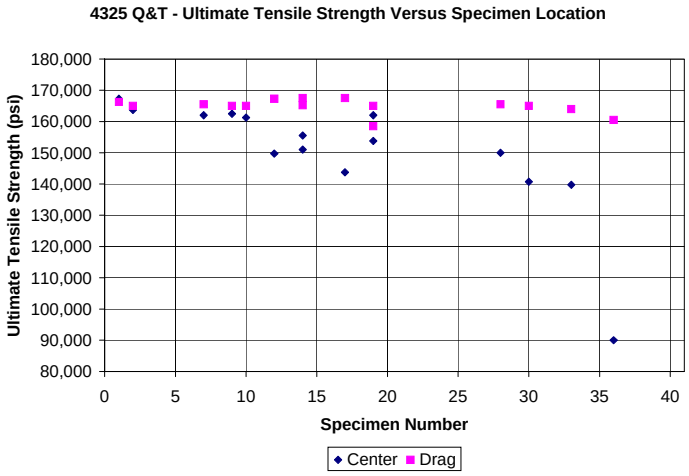

Figure 38. Relationship between ultimate tensile strength and specimen location in 4325Q&T.

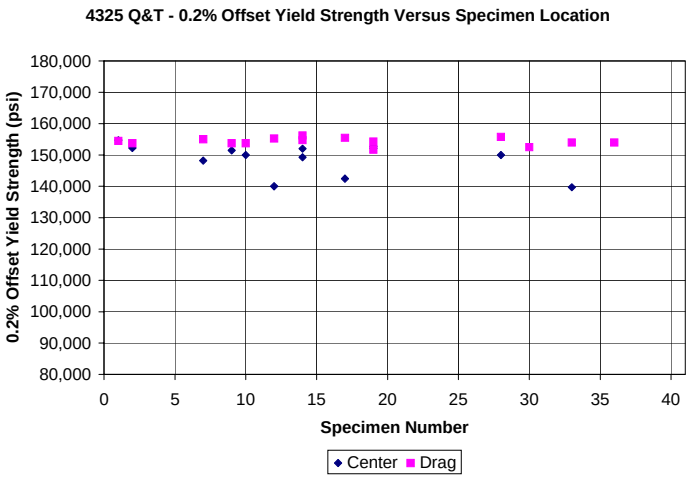

Figure 39. Relationship between yield strength and specimen location in 4325Q&T.

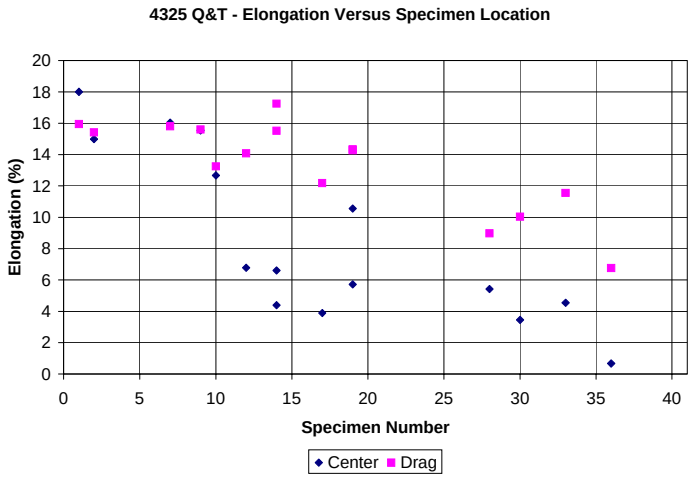

Figure 40. Relationship between elongation and specimen location in 4325Q&T.

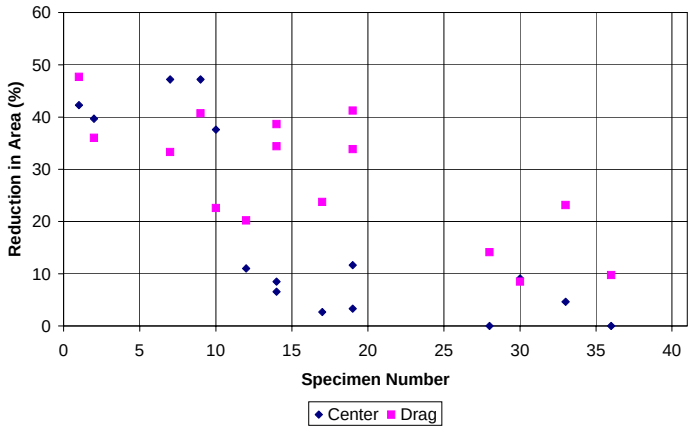

Figure 41. Relationship between reduction in area and specimen location in 4325Q&T.

Reduction of area ranged from 47% to 0% in the center samples and from 48% down to 10% in the drag samples.

A plot of fracture surface porosity versus specimen location is illustrated in Figure 42. As would be expected, the fracture surface porosity increased with increasing distance from the riser and porosity was higher in the center samples than in the drag samples. In the samples from the drag, the fracture surface porosity ranged from 0 to 15%, while in the center samples it ranged from 0 to 85%. Most of the highest fracture surface porosities were obtained in the samples located farthest from the riser and the highest was obtained in the center sample at sample position 36 with a fracture surface porosity of 85%.

A plot of Niyama porosity criterion and ultimate tensile strength as a function of specimen location for the 4325 quenched and tempered steel is illustrated in Figure 43. Ultimate and yield strengths were shown to be relatively insensitive to porosity so a Niyama value of around 0.7 or higher consistently produced ultimate strengths above 155,000 psi and yields above 150,000 psi. Below this value, the strengths were inconsistent.

Elongation and reduction were much more sensitive to the porosity in the castings so a Niyama value of greater than 2 was required to consistently produce elongation greater than 12% and reduction of area greater than 32% as illustrated in Figures 44 and 45. This would be expected since elongation and area reduction are much more sensitive to porosity than either ultimate or yield strength.

The tensile and yield strengths as a function of fracture surface porosity are plotted in Figure 46. Both the ultimate and yield strength remained fairly constant up to fracture surface porosities of about 20%. Values greater than 20% led to a decrease in both ultimate and yield strengths. The relationship between fracture surface porosity and elongation and reduction in area are illustrated in Figures 47 and 48. Similar to the 8630 steel, relatively small amounts of fracture surface porosity (<5%) decreases both elongation and reduction in area sharply.

The relationship between ultimate tensile strength and thru-transmission ultrasonic velocity is illustrated in Figure 49 and 50 for 2 and 5 MHz transducer frequencies. These plots include both the first break and second peak velocity measurements. At 2 MHz, the ultimate strength decreased rapidly at 2nd peak velocities lower than about 0.232 in/μsec. The first break velocity at 2 MHz had more scatter in the data but the data dropped off steeply at velocities below 0.2317 in/μsec. At 5 MHz, the first break data dropped off rapidly at velocities below 0.2319 in/μsec and the 2nd peak data dropped off at velocities below 0.2317 in/μsec. A similar set of plots for elongation as a function of thru transmission ultrasonic velocity is illustrated in Figures 51 and 52. At 2 MHz, higher elongations were associated with higher velocities over the entire range of elongations tested. At 5 MHz, there did not appear to be a correlation between elongation and velocity. For these steels, the 2 MHz thru transmission measurements appeared to give better indications of the strength and ductility results.

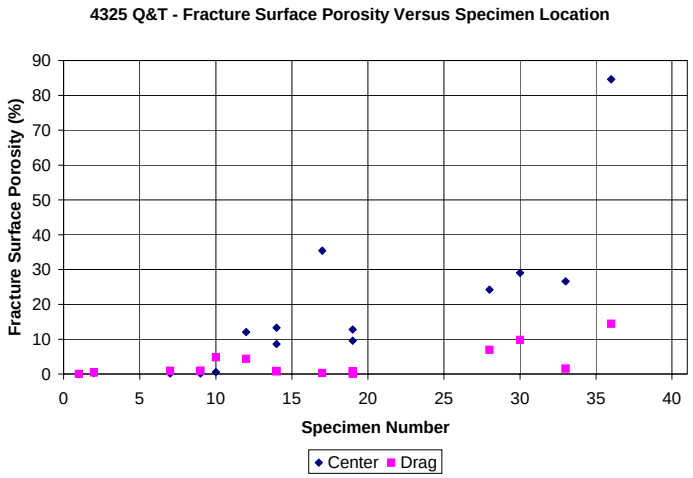

Figure 42. Relationship between fracture surface porosity and specimen location in 4325Q&T.

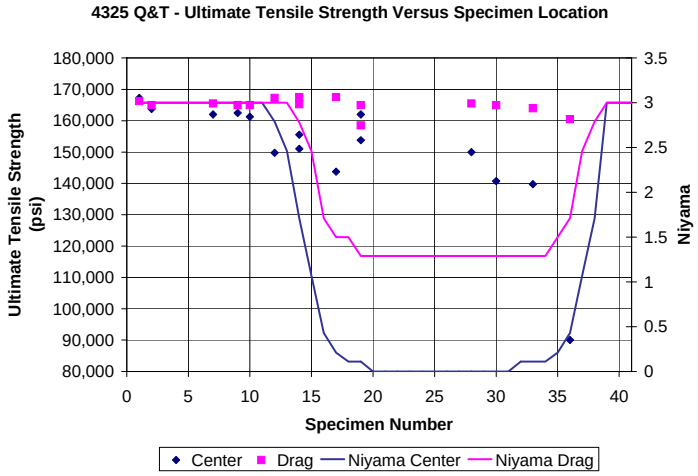

Figure 43. Relationship between ultimate tensile strength and Niyama in 4325Q&T.

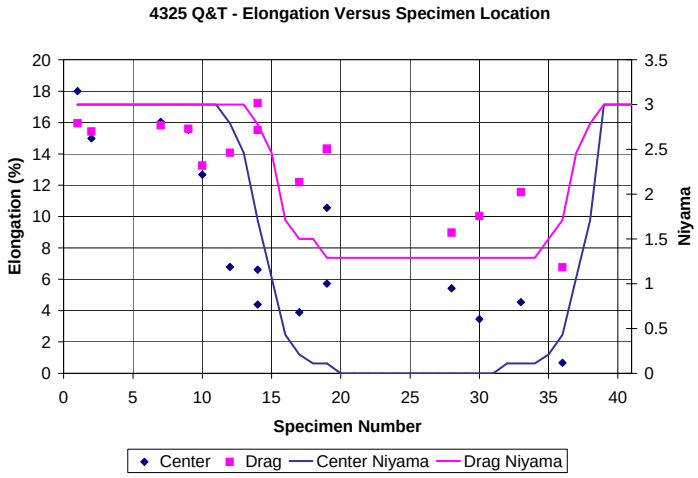

Figure 44. Relationship between elongation and Niyama in 4325Q&T.

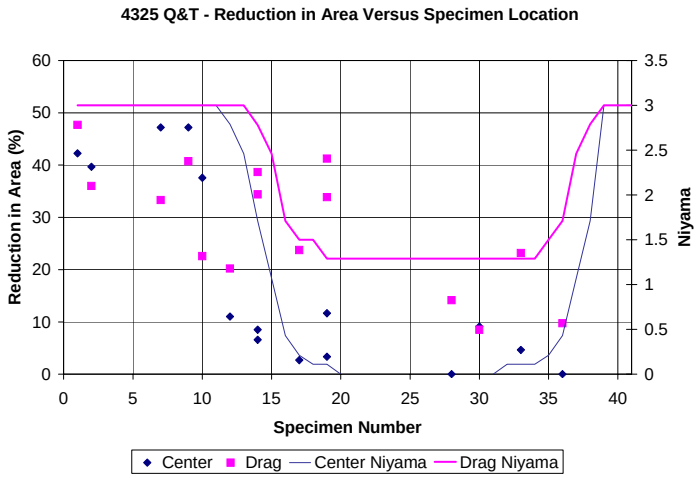

Figure 45. Relationship between reduction in area and Niyama in 4325Q&T.

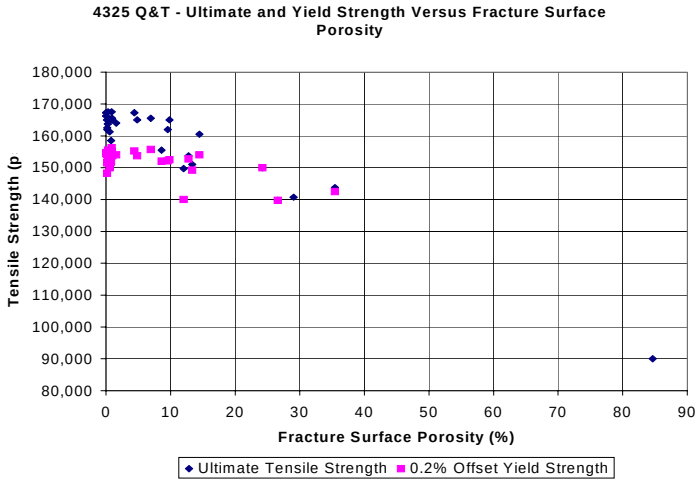

Figure 46. Relationship between tensile strength and fracture surface porosity in 4325Q&T.

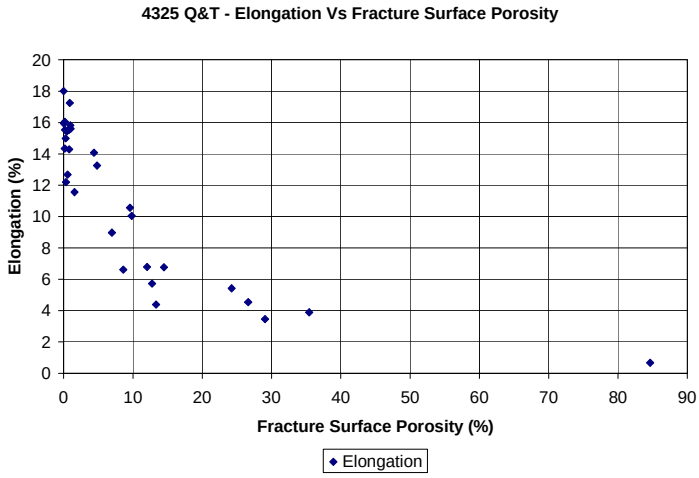

Figure 47. Relationship between elongation and fracture surface porosity in 4325Q&T.

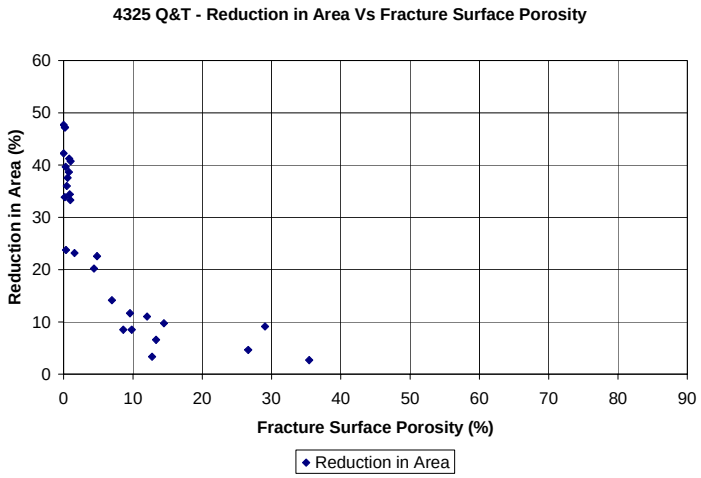

Figure 48. Relationship between reduction in area and fracture surface porosity in 4325Q&T.

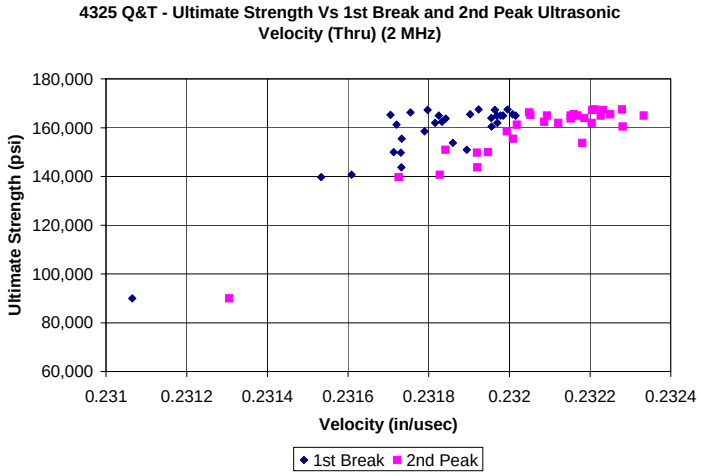

Figure 49. Relationship between ultimate strength and ultrasonic velocity in 4325Q&T (2 MHz).

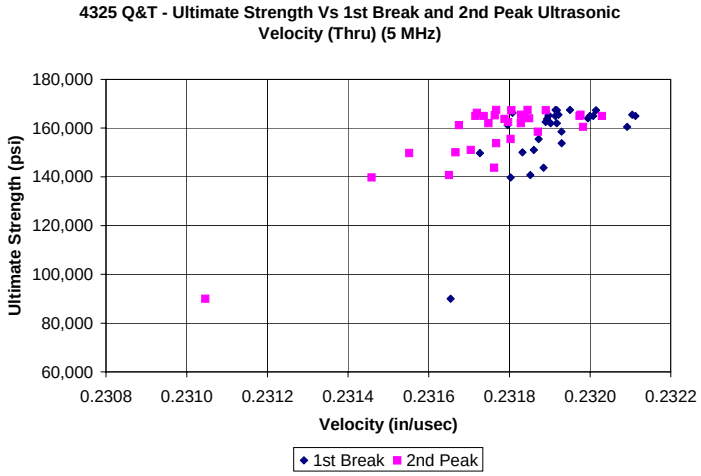

Figure 50. Relationship between ultimate tensile strength and ultrasonic velocity in 4325Q&T (5 MHz).

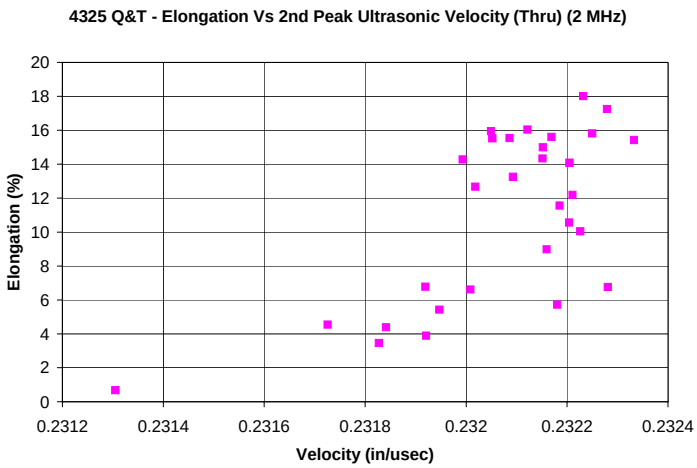

Figure 51. Relationship between elongation and ultrasonic velocity in 4325Q&T (2 MHz).

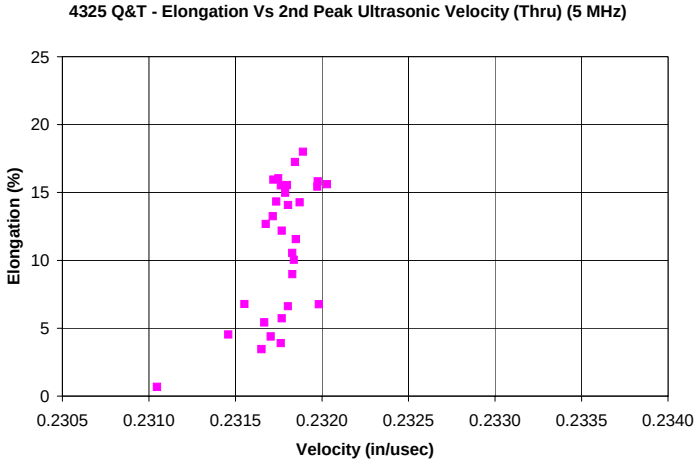

Figure 52. Relationship between elongation and ultrasonic velocity in 4325Q&T (5 MHz).

Attenuation on the tensile specimens was also measured in the thru transmission mode. Figure 53 and Figure 54 illustrates plots of both ultimate strength and percent elongation as a function of attenuation at 2 MHz. For the ultimate strengths, at back face signal strengths of less than about 65% there was a steep drop in the ultimate strength. Above this attenuation value, the ultimate strength was fairly constant. Elongation increased with increasing backface signal strength across the entire attenuation range. However, at signal strengths above 60% the results became much less predictable.

The ultimate and elongation versus the 2nd peak thru-back transmission velocity is illustrated in Figure 55 and 56 respectively. These graphs include the results for all three frequencies tested. At all three frequencies the ultimate strength response was relatively flat until the velocity dropped below a critical frequency. However, there was significant scatter in the results. Elongations showed an increase with increasing velocity at all three frequencies with significant scatter over the entire velocity range.

Tensile strength and elongation versus thru-back transmission attenuation is illustrated in Figure 57 and 58. At 10 MHz when attenuation increased above about 1.25 dB/inch the ultimate strength started to decrease. A similar result was shown at 2 and 5 MHz at about 1.5 db/inch. The scatter was lower at 2 and 5 MHz than was seen at 10 MHz. Elongations decreased with increasing attenuation with significant scatter in the data at values below about 1.5 db/inch.

3.1.3 CA6NM

A plot of all tensile stress/strain curves to failure is shown in Figure 59. Specimens containing large amounts of porosity can be readily identified by their low strain values. Tensile strengths ranged from 75,000 psi up to 119,000 while yield strengths ranged from 64,000 to 80,000 psi. The largest variation was seen in the reduction of area which ranged from 17.6 up to 57.6%. Elongation values ranged from a low of 6.4% up to 28.9%. The lowest tensile properties were measured in the specimens removed from the center section, as would be expected since that is the most likely location for shrinkage to form.

In Figure 60, the ultimate tensile strength versus specimen location in the casting is illustrated. In the drag samples, there was little variation in the tensile strength along the length of the bar. Values ranged from 114,200 up to 118,200 psi. In the center specimens, the ultimate strength began to drop at position 9, which was located a few inches from the right side of the riser. The ultimate strength ranged from 80,000 to 114,000 psi in the center of the casting.

The yield strength versus sample location is illustrated in Figure 61. The range in yield strength from the drag was narrow as compared to the ultimate strength and only ranged from 75,800 up to 80,000 psi. There was more scatter in the samples from the center although there did not appear to be any relationship between yield and sample location. The yield in the center samples ranged from 79,400 up to 80,000 psi.

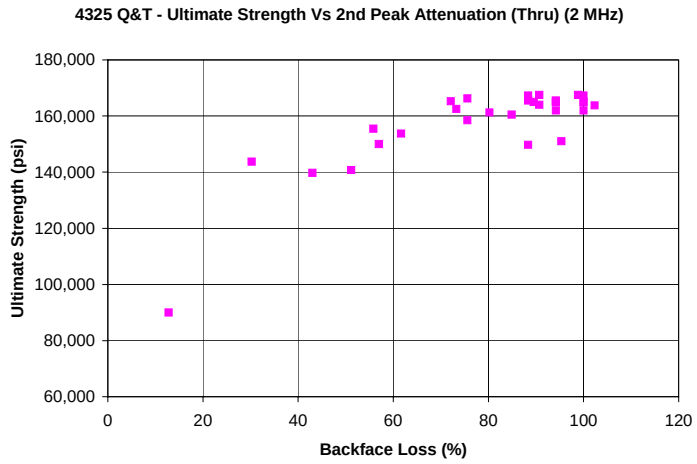

Figure 53. Relationship between ultimate tensile strength and ultrasonic backface in 4325Q&T (2 MHz).

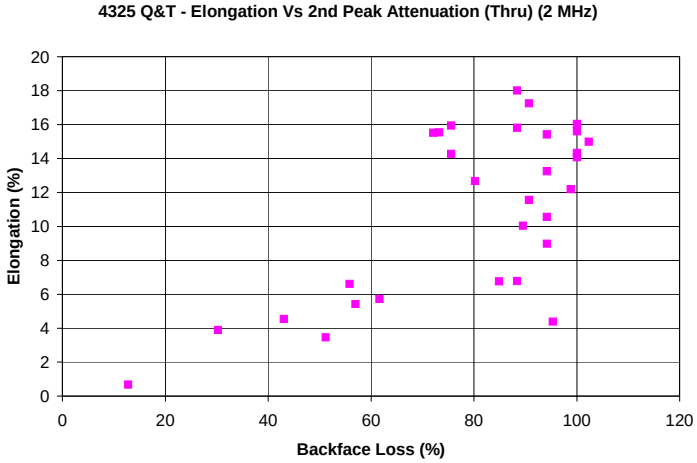

Figure 54. Relationship between elongation and ultrasonic backface in 4325Q&T (2 MHz).

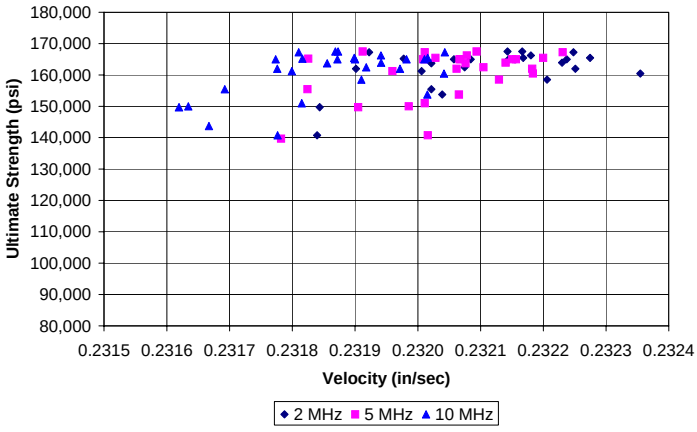

Figure 55. Relationship between ultimate tensile strength and ultrasonic velocity in 4325Q&T.

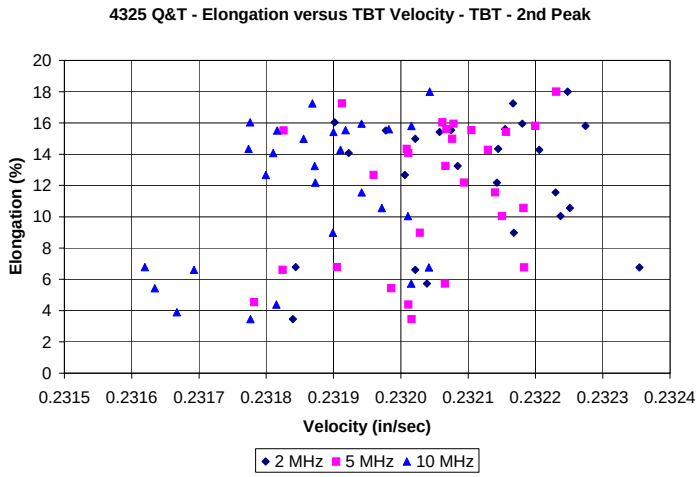

Figure 56. Relationship between elongation and ultrasonic velocity in 4325Q&T.

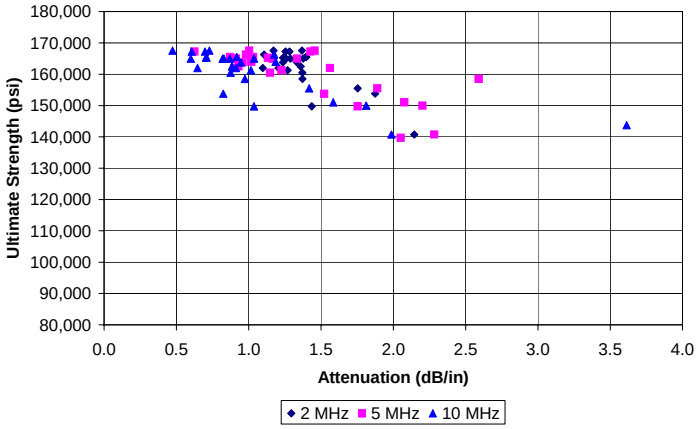

Figure 57. Relationship between ultimate tensile strength and ultrasonic attenuation in 4325Q&T.

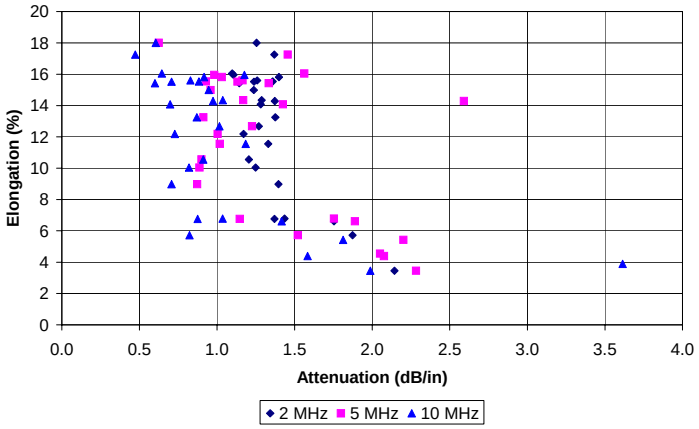

Figure 58. Relationship between elongation and ultrasonic attenuation in 4325Q&T.

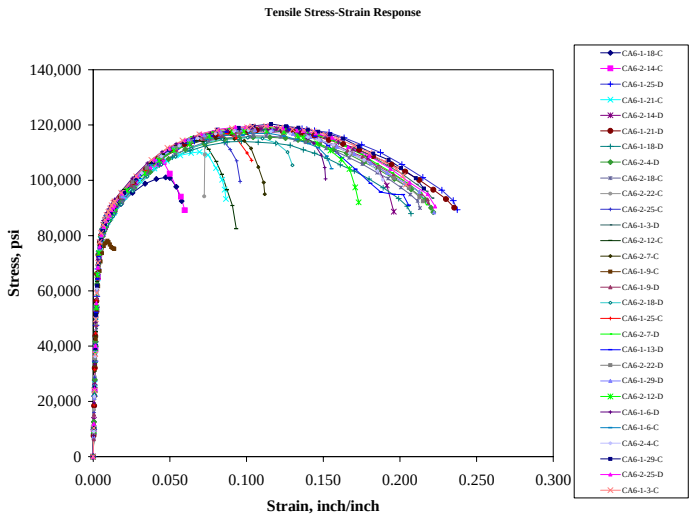

Figure 59. Tensile stress-strain curves for CA6NM cast steel.

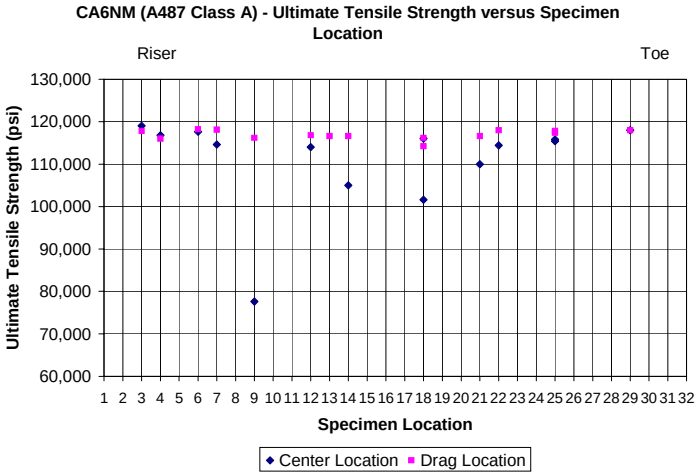

Figure 60. Relationship between ultimate tensile strength and specimen location in CA6NM.

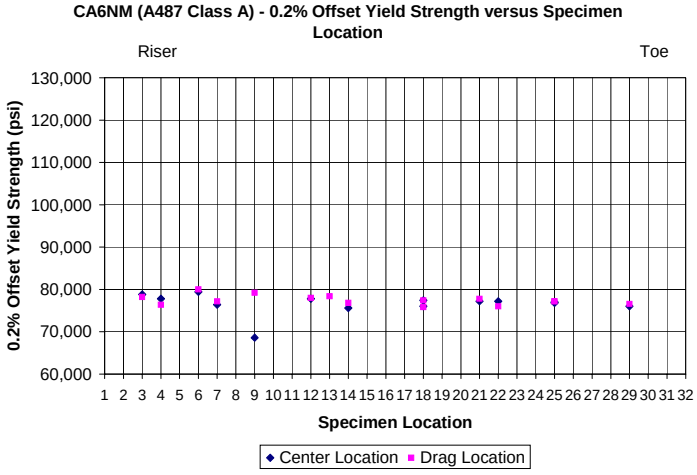

Figure 61. Relationship between yield strength and specimen location in CA6NM.

Plots for elongation and reduction of area versus specimen location are illustrated in Figures 62 and 63, respectively. Both the center and drag samples showed a drop in ductility and reduction in area as the distance from the riser increased. The drop in elongation and reduction in area was greater in the center samples than in the drag samples and this is probably due to higher porosity content in these samples. The percent elongation was about 23.0% near the riser and 6.4% in the center samples while it ranged from 13.8 to 28.9% in the drag samples. Reduction of area ranged from 17.6% to 54.2% in the center samples and from 27.8% down to 54.6% in the drag samples.

A plot of fracture surface porosity versus specimen location is illustrated in Figure 64. As would be expected, the fracture surface porosity increased with increasing distance from the riser and porosity was higher in the center samples than in the drag samples. In the samples from the drag, the fracture surface porosity ranged from 0 to 10.9%, while in the center samples it ranged from 0 to 49.5%.

A plot of Niyama porosity criterion and tensile strength as a function of specimen location for the CA6NM steel is illustrated in Figure 65. Ultimate and yield strengths were shown to be relatively insensitive to porosity so a Niyama value of around 0.7 or higher consistently produced ultimate strengths above 115,000 psi and yields above 75,000 psi. Below this value, the strengths were inconsistent.

Elongation and reduction were much more sensitive to the porosity in the castings so a Niyama value of greater than 1.4 was required to consistently produce elongation greater than 20% and reduction of area greater than 40% as illustrated in Figures 66 and 67. This would be expected since elongation and area reduction are much more sensitive to porosity than either ultimate or yield strength.

The tensile and yield strengths as a function of fracture surface porosity are plotted in Figure 68. Both the ultimate and yield strength remained fairly constant up to fracture surface porosities of about 15%. Values greater than 15% led to a decrease in both ultimate and yield strengths. The relationship between fracture surface porosity and elongation and reduction in area are illustrated in Figures 69 and 70. Similar to the 8630 and 4325 steels, relatively small amounts of fracture surface porosity (<5%) decreases both elongation and reduction in area sharply.

Traditionally, high alloys steels cannot be tested ultrasonically due to the high attenuation caused by the microstructure. Comparisons of ultrasonic velocities and mechanical properties were non-discriminatory.

3.1.4 CD3MN

A plot of all tensile stress/strain curves to failure is shown in Figure 71. Specimens containing large amounts of porosity can be readily identified by their low strain values. Tensile

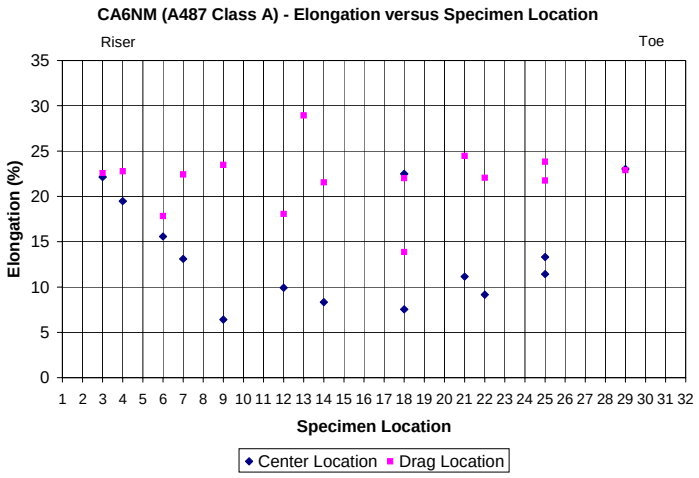

Figure 62. Relationship between elongation and specimen location in CA6NM.

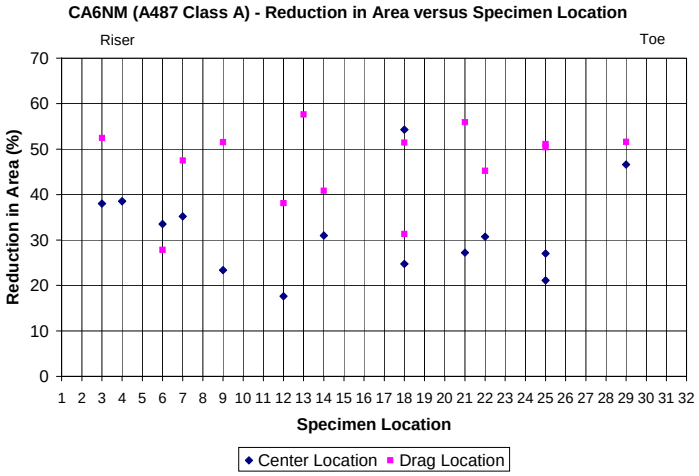

Figure 63. Relationship between reduction in area and specimen location in CA6NM.

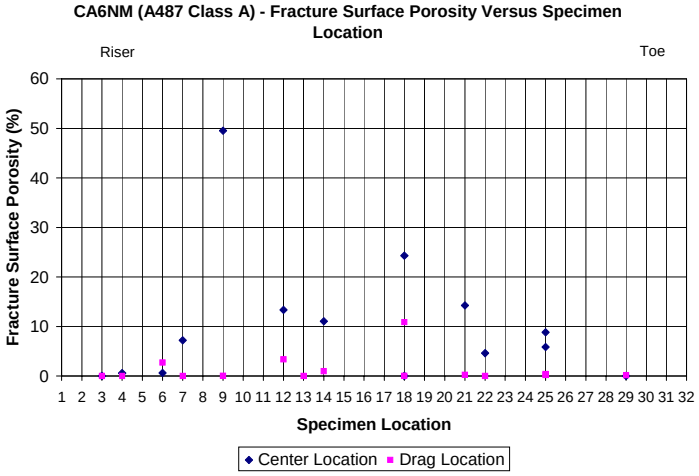

Figure 64. Relationship between fracture surface porosity and specimen location in CA6NM.

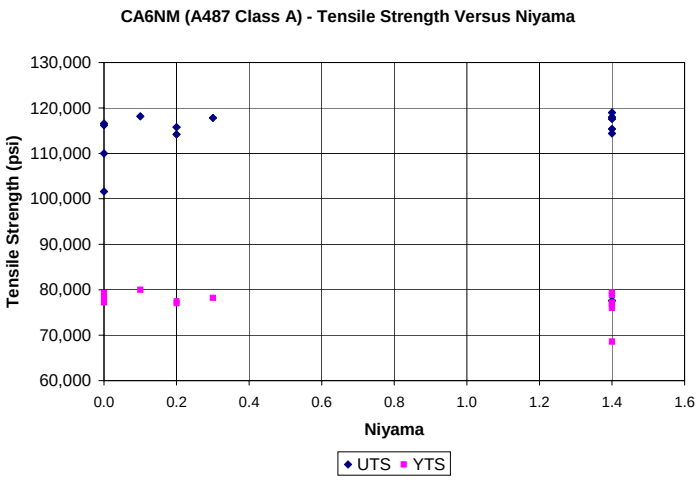

Figure 65. Relationship between tensile strength and Niyama in CA6NM.

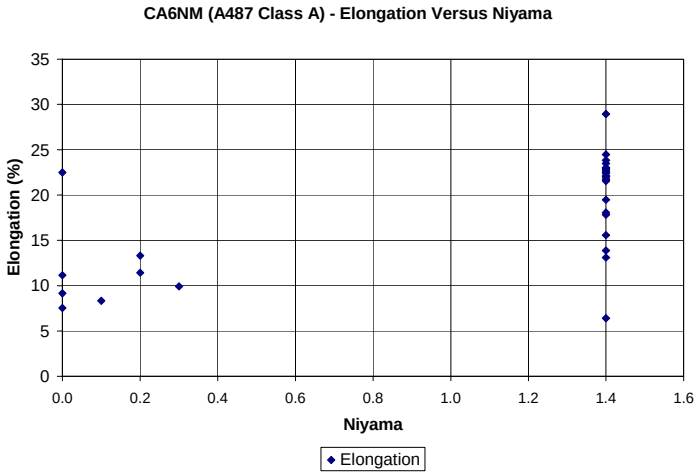

Figure 66. Relationship between elongation and Niyama in CA6NM.

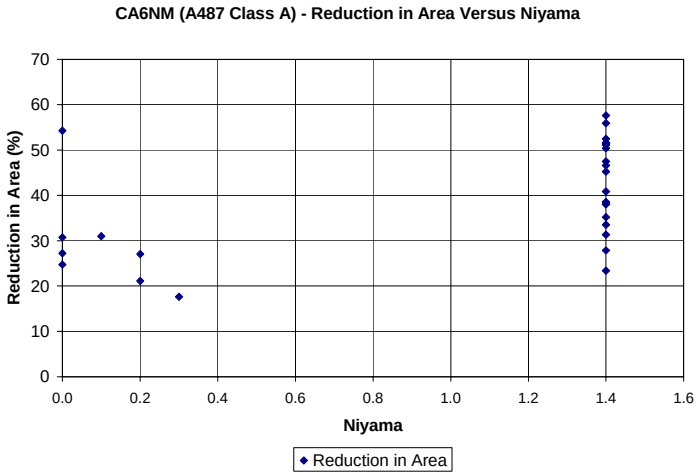

Figure 67. Relationship between elongation and Niyama in CA6NM.

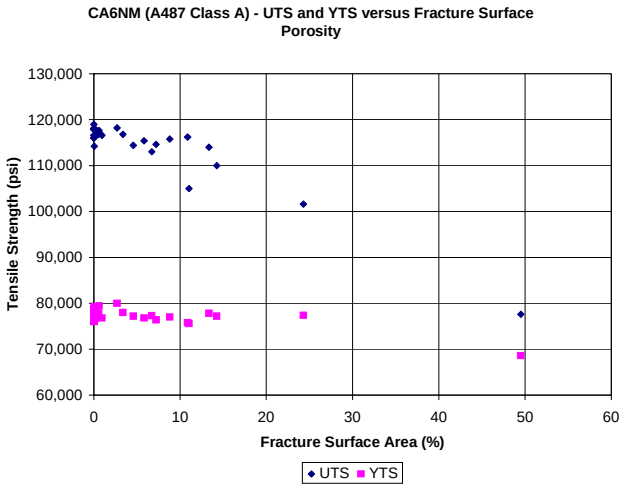

Figure 68. Relationship between tensile strength and fracture surface porosity in CA6NM.

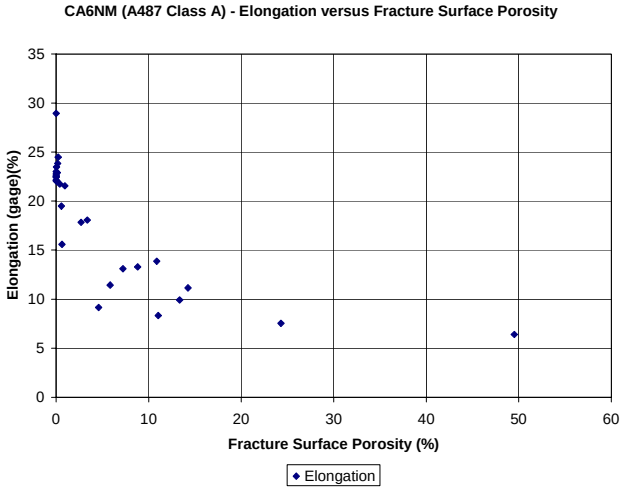

Figure 69. Relationship between elongation and fracture surface porosity in CA6NM.

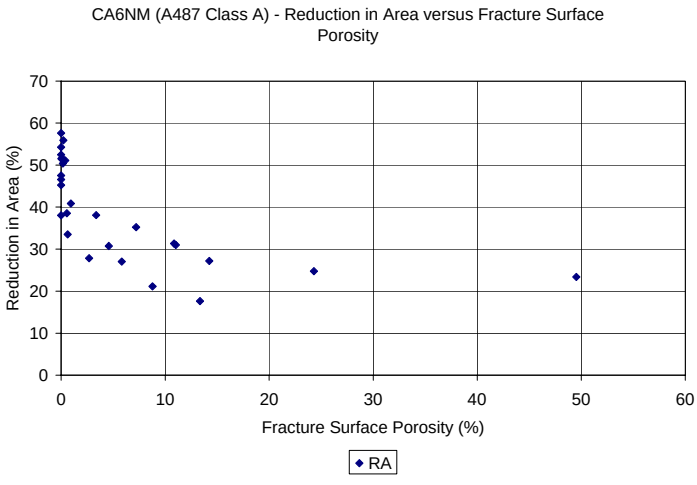

Figure 70. Relationship between reduction in area and fracture surface porosity in CA6NM.

strengths ranged from 75,000 psi up to 103,800 while yield strengths ranged from 63,400 to 77,600 psi. The largest variation was seen in the reduction of area, which ranged from 33.1 up to 74.1%. Elongation values ranged from a low of 3.5% up to 43.5%. The lowest tensile properties were measured in the specimens removed from the center section, as would be expected since that is the most likely location for shrinkage to form.

In Figure 72, the ultimate tensile strength versus specimen location in the casting is illustrated. In the drag samples, there was little variation in the tensile strength along the length of the bar. Values ranged from 103,800 up to 94,000 psi. In the center specimens, the ultimate strength began to drop at position 8, which was located a few inches from the right side of the riser. The ultimate strength ranged from 75,000 to 101,400 psi in the center of the casting.

The yield strength versus sample location is illustrated in Figure 73. The range in yield strength from the drag was narrow as compared to the ultimate strength and only ranged from 63,400 up to 77,600 psi. There was more scatter in the samples from the center although there did not appear to be any relationship between yield and sample location. The yield in the center samples ranged from 66,600 up to 77,600 psi.

Plots for elongation and reduction of area versus specimen location are illustrated in Figures 74 and 75, respectively. Both the center and drag samples showed a drop in ductility and reduction in area as the distance from the riser increased. The drop in elongation and reduction in area was greater in the center samples than in the drag samples and this is due to higher porosity content in these samples. The percent elongation was about 38.6% near the riser and 3.5% in the center samples while it ranged from 18.2 to 43.5% in the drag samples. Reduction of area ranged from 33.2% to 72.4% in the center samples and from 34.9% down to 74.1% in the drag samples.

A plot of Niyama porosity criterion and tensile strength as a function of specimen location for the CD3MN steel is illustrated in Figure 76. Ultimate and yield strengths were shown to be relatively insensitive to porosity so a Niyama value of around 0.7 or higher consistently produced ultimate strengths above 95,000 psi and yields above 70,000 psi. Below this value, the strengths were inconsistent.

Elongation and reduction were much more sensitive to the porosity in the castings so a Niyama value of greater than 1.4 was required to consistently produce elongation greater than 30% and reduction of area greater than 60% as illustrated in Figures 77 and 78. This would be expected since elongation and area reduction are much more sensitive to porosity than either ultimate or yield strength.

The tensile and yield strengths as a function of fracture surface porosity are plotted in Figure 79. Both the ultimate and yield strength remained fairly constant up to fracture surface porosities of about 20%. Values greater than 20% led to a decrease in both ultimate and yield strengths. The relationship between fracture surface porosity and elongation and reduction in

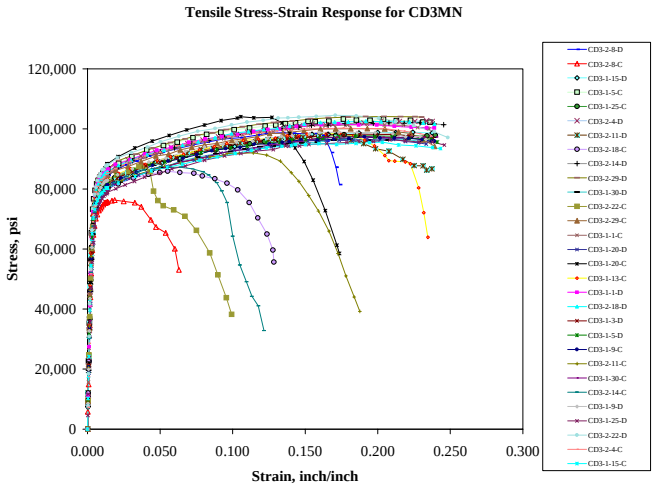

Figure 71. Tensile stress-strain curves for CD3MN cast steel.

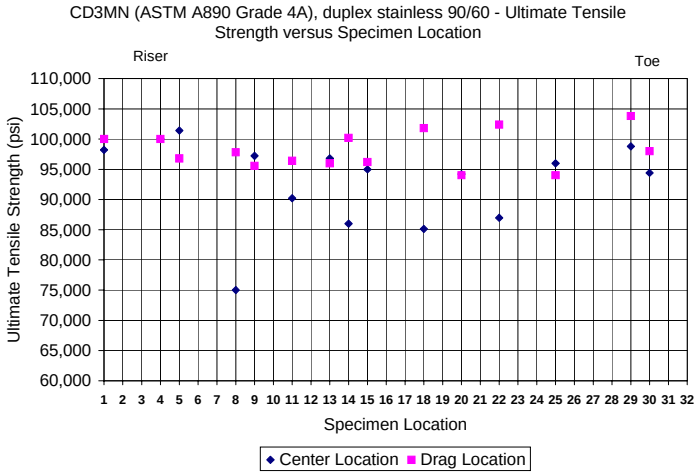

Figure 72. Relationship between ultimate tensile strength and specimen location in CD3MN.

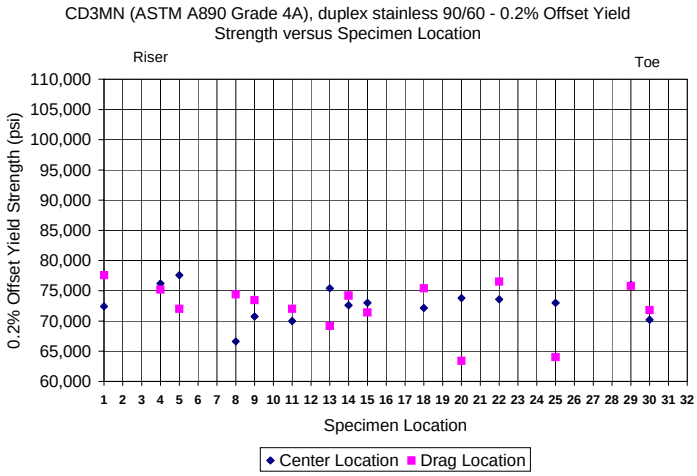

Figure 73. Relationship between yield strength and specimen location in CA6NM.

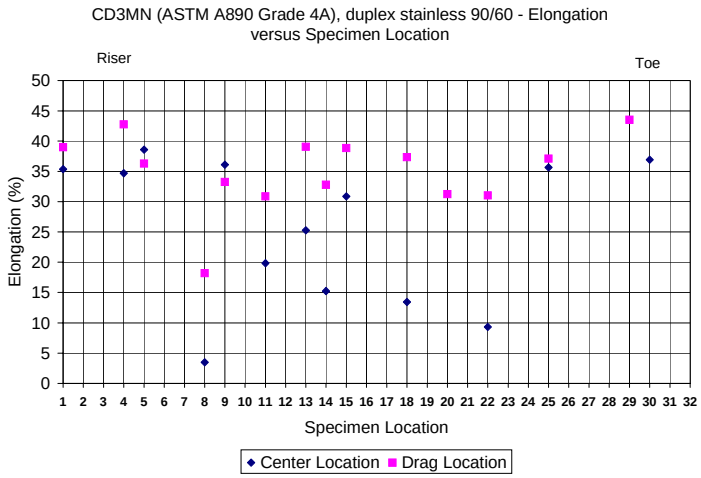

Figure 74. Relationship between elongation and specimen location in CD3MN.

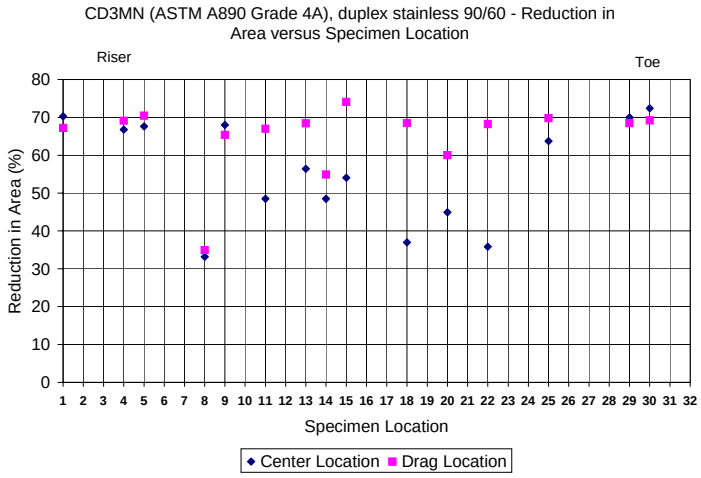

Figure 75. Relationship between reduction in area and specimen location in CD3MN.

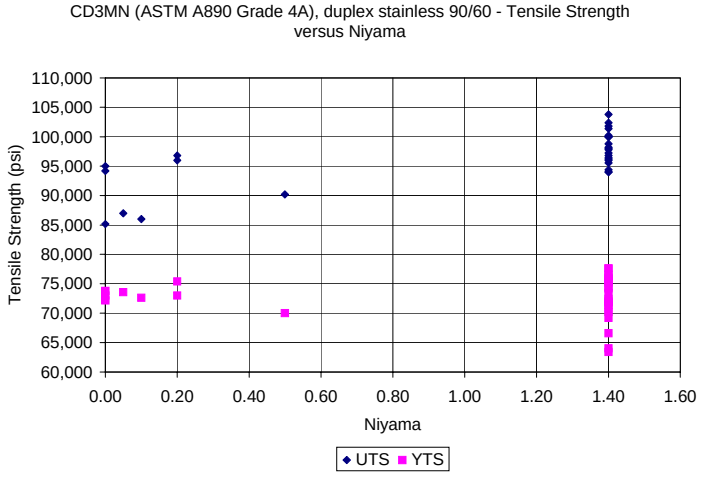

Figure 76. Relationship between tensile strength and Niyama in CD3MN.

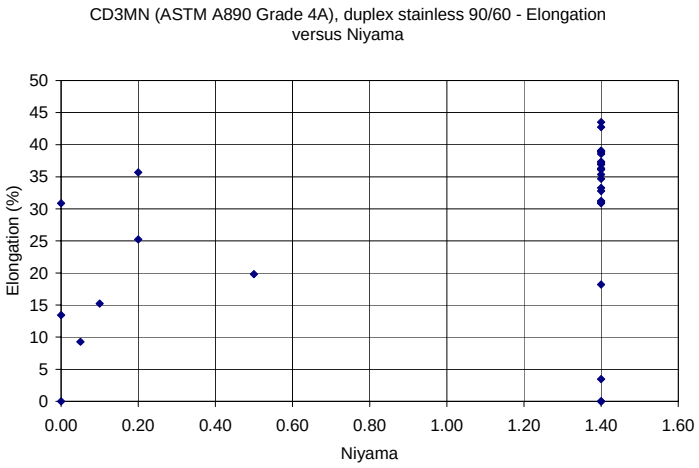

Figure 77. Relationship between elongation and Niyama in CD3MN.

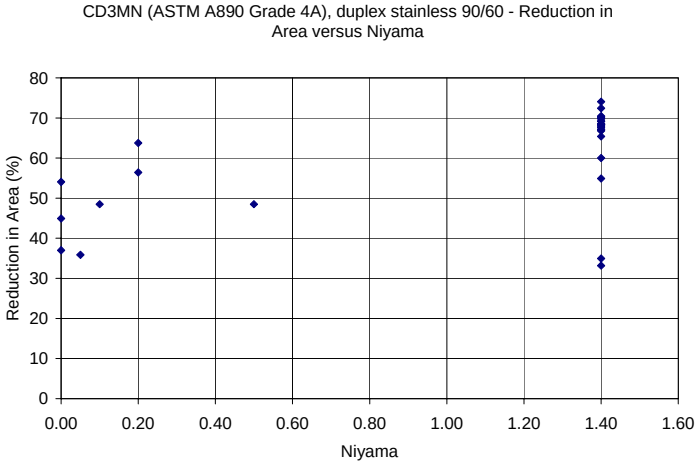

Figure 78. Relationship between reduction in area and Niyama in CD3MN.

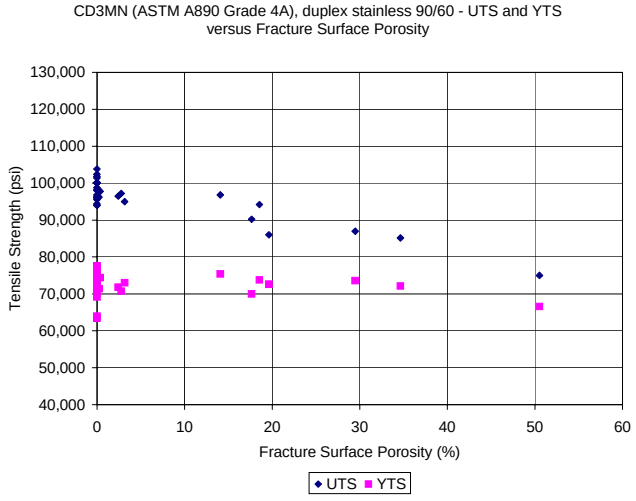

Figure 79. Relationship between tensile strength and fracture surface porosity in CD3MN.

area are illustrated in Figures 80 and 81. Similar to the 8630 and 4325 steels, relatively small amounts of fracture surface porosity (<5%) decreases both elongation and reduction in area but the decrease is much more gradual due to the high ductility of this alloy.

Traditionally, high alloys steels cannot be tested ultrasonically due to the high attenuation caused by the microstructure. Comparisons of ultrasonic velocities and mechanical properties were non-discriminatory.

3.2 CHARPY DATA

3.2.1 8630 Quenched and Tempered Cast Steel

The relationship between Charpy impact values and specimen location is illustrated in Figure 82. While higher impact values are observed in the toe of the casting, the remaining values are consistent across the plate. Figure 83 plots lateral expansion versus specimen location. Similar to the impact values, lateral expansion was consistent across the plate. Fracture surface porosity does not vary much, with two exceptions that do not correlate with a decrease in properties, as shown in Figure 84.

Figure 85 illustrates the correlation between fracture surface porosity and Charpy impact values at -40°F. Unlike tensile properties, the correlation between fracture surface porosity and Charpy impact values is weak at best. This is primarily due to the nature of the test. In a tensile test, the load is applied to a volume at a relatively low rate. Cracks will initiate at anomalies, such as shrink pores, and extend. The local area stress will start increasing again until the yield point is exceeded, the crack will extend again and the process is repeated. At some point, cracks will start linking up forming larger cracks and the specimen will fail by net section loss. With a Charpy impact test, the loading is much faster and is not applied to a significant volume. Cracks do not have time to form and link up as in a tensile test. The plane of highest stress is not dictated by the crack forming anomalies in the metal but by the notch cut into the specimen. So crack forming porosity should have some but not a large effect on Charpy impact properties.

3.2.2 4325 Quenched and Tempered Cast Steel

The correlation between Charpy impact energy and lateral expansion values at -40°F and specimen location is illustrated in Figures 86 and 87 respectively. There may be a slight decrease in impact energy and lateral expansion as the distance from the riser increased, but unlike tensile properties, the correlation between fracture surface porosity and Charpy impact values is weak at best. This is primarily due to the nature of the test. In a tensile test, the load is applied to a volume at a relatively low rate. Cracks will initiate at anomalies, such as shrink pores, and extend. The local area stress will start increasing again until the yield point is exceeded, the crack will extend again and the process is repeated. At some point, cracks will start linking up forming larger cracks and the specimen will fail by net section loss. With a Charpy impact test, the loading is much faster and is not applied to a significant volume. Cracks do not have time to

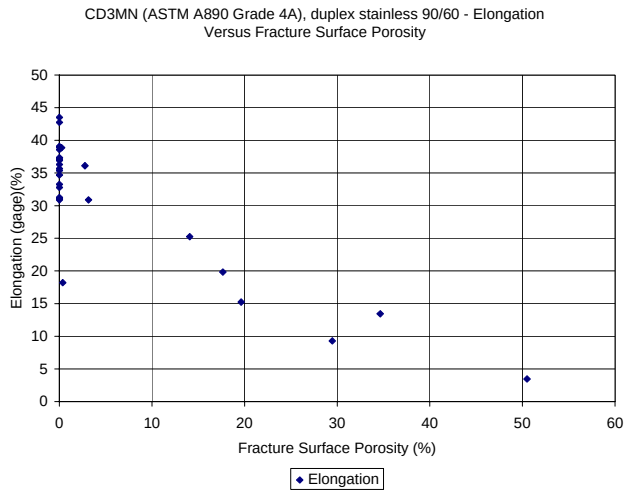

Figure 80. Relationship between elongation and fracture surface porosity in CD3MN.

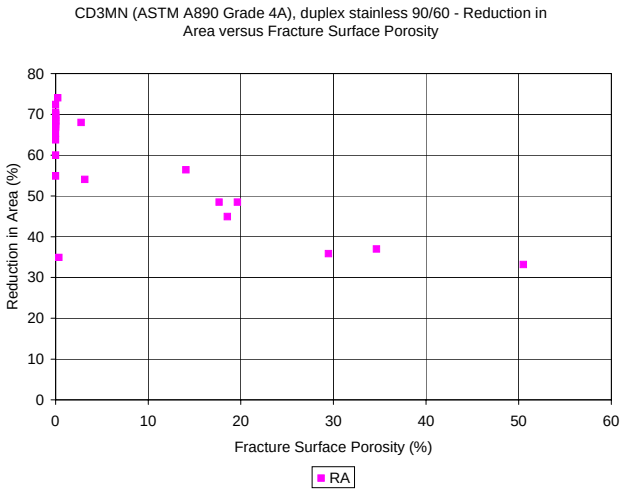

Figure 81. Relationship between reduction in area and fracture surface porosity in CD3MN.

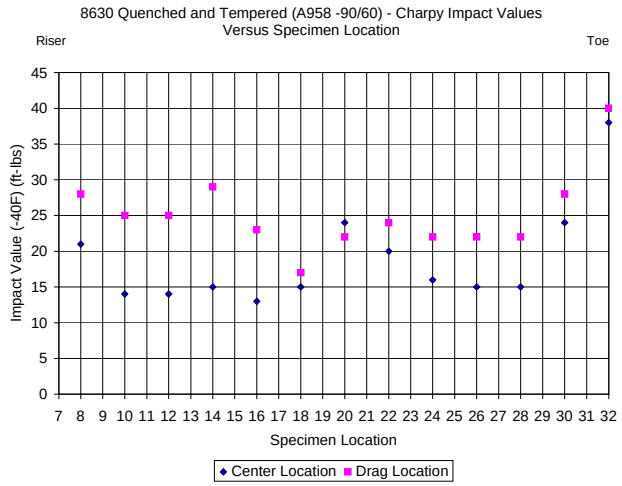

Figure 82. Relationship between Charpy impact values and specimen location in 8630Q&T.

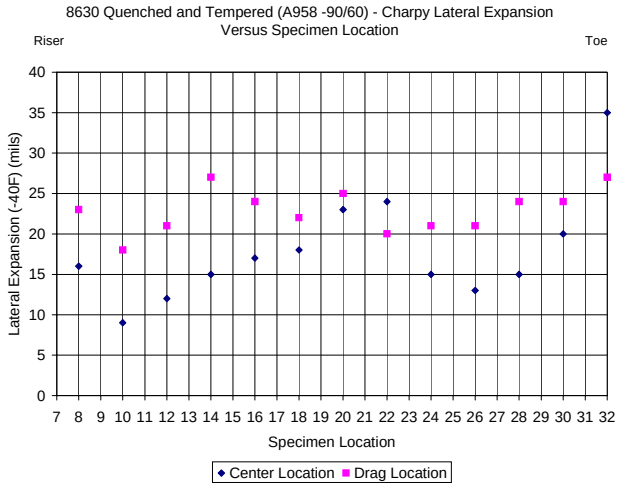

Figure 83. Relationship between Charpy lateral expansion and specimen location in 8630Q&T.

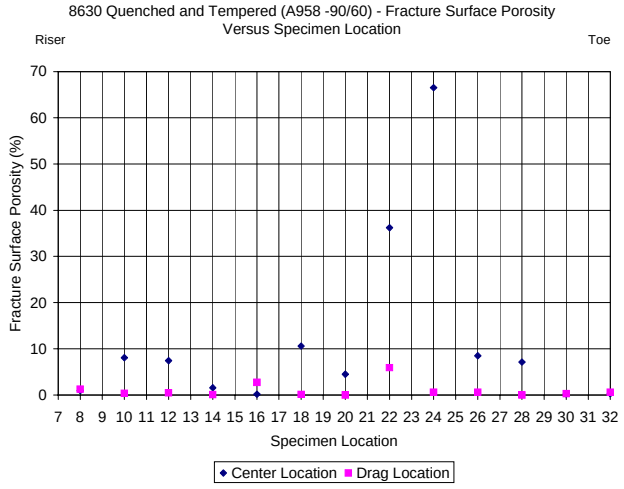

Figure 84. Relationship between fracture surface porosity and specimen location in 8630Q&T.

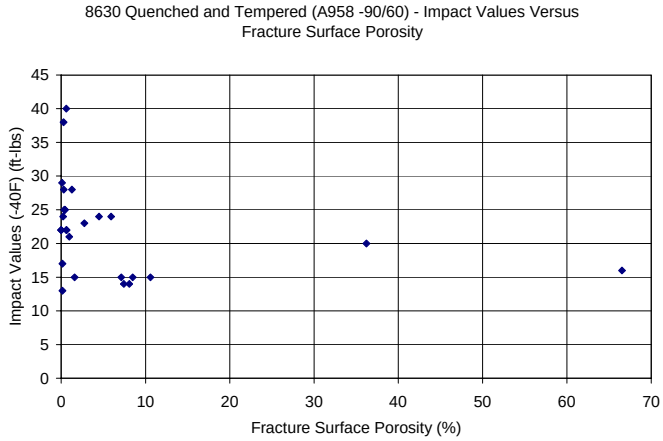

Figure 85. Relationship between Charpy impact values and fracture surface porosity in 8630Q&T.

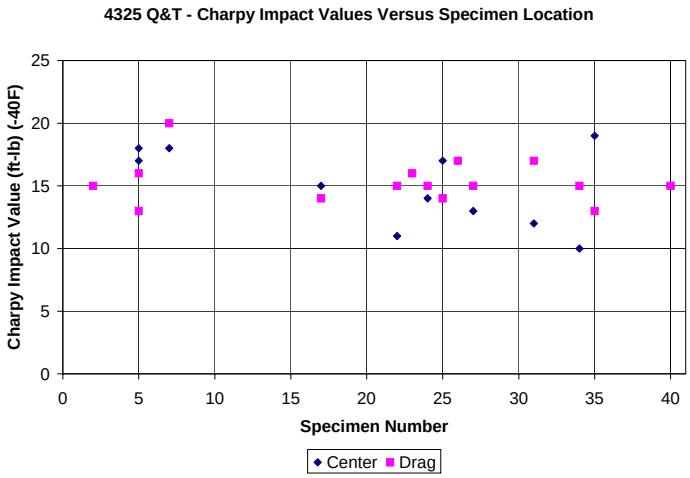

Figure 86. Relationship between Charpy impact values and specimen location in 4325Q&T.

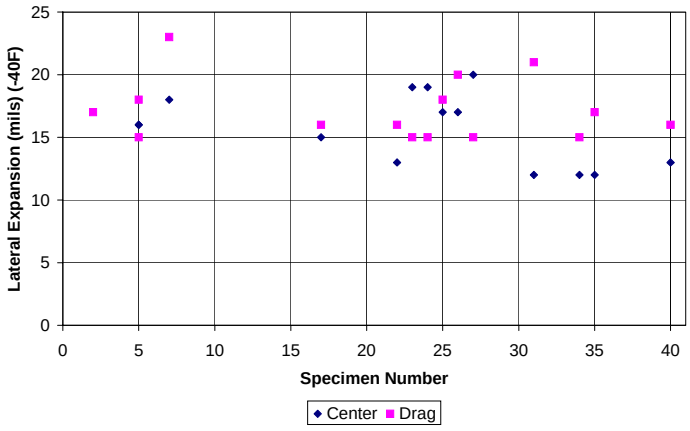

Figure 87. Relationship between Charpy lateral expansion values and specimen location in 4325Q&T.

form and link up as in a tensile test. The plane of highest stress is not dictated by the crack forming anomalies in the metal but by the notch cut into the specimen. Therefore, crack forming porosity should have some but not a large effect on Charpy impact properties.

3.3 MICROSTRUCTURAL DATA

Sections were removed from tested tensile specimens from all four alloys for metallurgical inspection. The sections were perpendicular to the stress direction to reveal any porosity that the stress field would interact upon and were as close to the fracture surface as possible. The objective was to determine if a correlation could be revealed between fracture surface porosity, which has consistently demonstrated a correlation to tensile properties in a range of steel casting alloys, to metallurgical porosity which is commonly measured in the field and is detected by non-destructive tests. Two restrictions were likely with this procedure – the fracture may contain the highest volume of porosity and could not be measured, and the non-uniform nature of shrink porosity in metals makes the statistical probability of polishing through a high porosity area quite low. However, the experiment may provide useful information for future research.

The relationship between fracture surface porosity and metallurgical cluster porosity in 8630 quenched and tempered steel is illustrated in Figure 88. While the plot contains considerable data scatter, as was expected, the plot trends toward a fracture to metallurgical porosity ratio of about 4-6 to 1, which is in line with previous work. Figure 89 illustrates the correlation between tensile strength and metallurgical porosity. The ultimate tensile strength trends toward lower values after metallurgical porosity increases pass about 5%, which matches well with a fracture surface value of about 20-30% where strength values were observed to decrease.

The relationship between fracture surface porosity and metallurgical cluster porosity in 4325 quenched and tempered steel is illustrated in Figure 90. While the plot contains considerable data scatter, as was expected, the plot trends toward a fracture to metallurgical porosity ratio of about 4-6 to 1, similar to the 8630 data. Figure 91 illustrates the correlation between tensile strength and metallurgical porosity. The ultimate tensile strength trends toward lower values after metallurgical porosity increases to 2-4%, which matches well with a fracture surface value of about 20% where tensile strength values were observed to decrease.

The relationship between fracture surface porosity and metallurgical cluster porosity in 4325 quenched and tempered steel is illustrated in Figure 90. While the plot contains considerable data scatter, as was expected, the plot trends toward a fracture to metallurgical porosity ratio of about 4-6 to 1, similar to the 8630 data. Figure 91 illustrates the correlation between tensile strength and metallurgical porosity. The ultimate tensile strength trends toward lower values after metallurgical porosity increases to 2-4%, which matches well with a fracture surface value of about 20% where tensile strength values were observed to decrease.

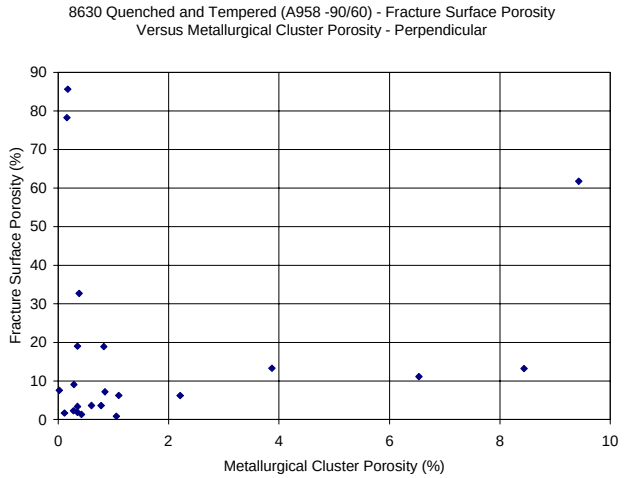

Figure 88. Relationship between fracture surface porosity and cluster porosity in 8630Q&T.

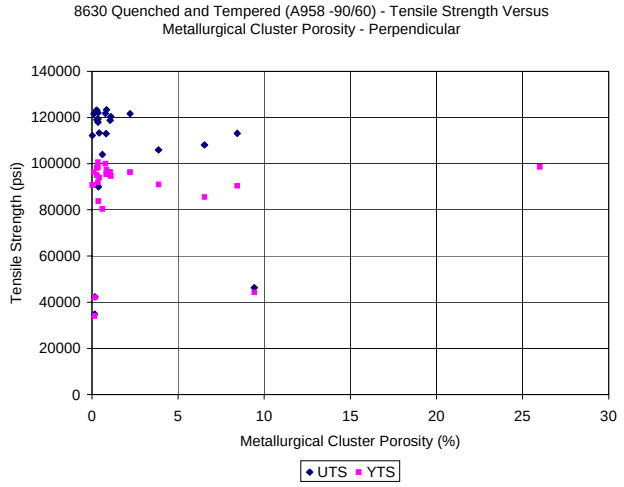

Figure 89. Relationship between tensile strength and cluster porosity in 8630Q&T.

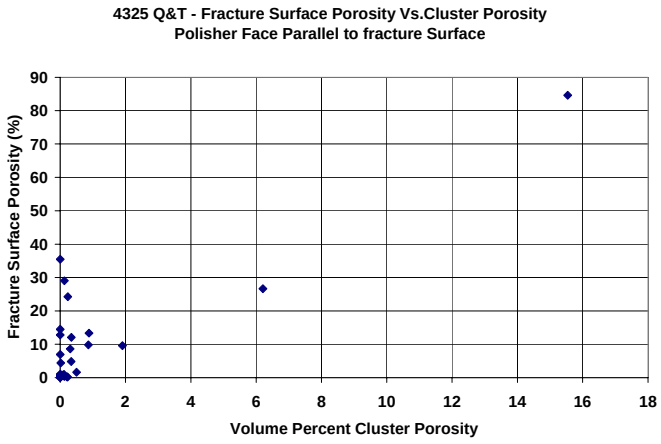

Figure 90. Relationship between fracture surface porosity and cluster porosity in 4325Q&T.

The relationship between fracture surface porosity and metallurgical cluster porosity in CA6NM steel is illustrated in Figure 92. This data does not show any reasonable correlation between the two measurements. Figure 93 illustrates the correlation between tensile strength and metallurgical porosity. Again, a reasonable correlation does not exist with this data. This high alloy steel has a significantly higher ductility and fracture toughness compared to the 8630 and 4325 steels. The damage tolerant nature of the CA6NM may make the correlation less likely to detect with this method. Also, high alloys have a longer solidification range which may change the shape of the porosity but no necessarily the volume. Instead of a cluster of micro-pores that might exist in a shorter freezing alloy, an alloy with a longer freezing range would allow any shrink porosity to form fewer single large cavities which would appear on the fracture face, not in the metallurgical measurement.

The relationship between fracture surface porosity and metallurgical cluster porosity in CD3MN steel is illustrated in Figure 94. This data is very similar to the CA6NM data for the same reasons. Figure 95 illustrates the correlation between tensile strength and metallurgical porosity. Again, a reasonable correlation does not exist with this data for the same reasons as the CA6NM steel.

4. COMPARISON OF ALL ALLOYS

The response of ultimate strength, elongation, and reduction in area were very similar in all four alloys to micro-porosity. Several plots were produced to illustrate this similarity in response. The strength values and fracture toughness values for these alloys varied widely so the strengths were normalized by taking the ratio of the ultimate and yield strength and dividing by the K_{Ic} fracture toughness value.

The relationship between the ultimate strength of all alloys tested and specimen location is illustrated in Figure 96. The specimen location was normalized to account for some variation in plate length. This same data is plotted using normalized strength data in Figure 97. The lower tensile values were skewed closer to the riser side of the plate than the toe of the test plate illustrating the solidification profile introduced by the ingate located in the riser.

Fracture surface has a uniform effect on ultimate tensile strength as can be observed in Figure 98. All four alloy show a decrease in tensile strength at fracture surface porosity values of about 20%. Figure 99 illustrates this same trend after the strength data has been normalized. Reduction in area and elongation values show some similarity but also some differences in these alloy, as shown in Figure 100. All alloys show a decrease in elongation with relatively small amounts of fracture surface porosity although the rate of decrease is not the same. The higher ductility alloys less sensitive to fracture surface porosity compared the higher strength, lower ductility alloys.

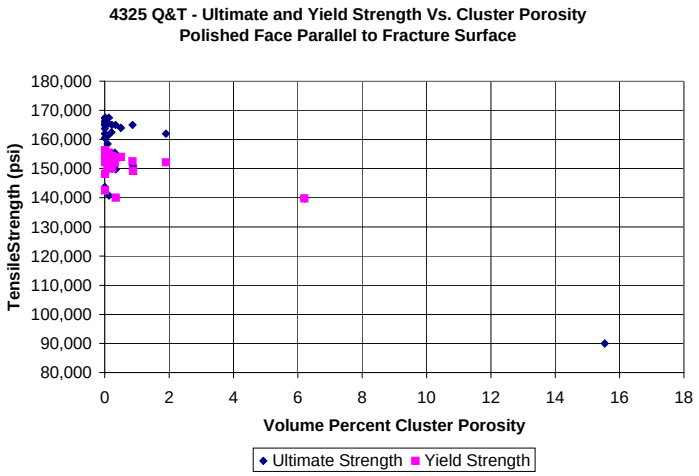

Figure 91. Relationship between tensile strength and cluster porosity in 4325Q&T.

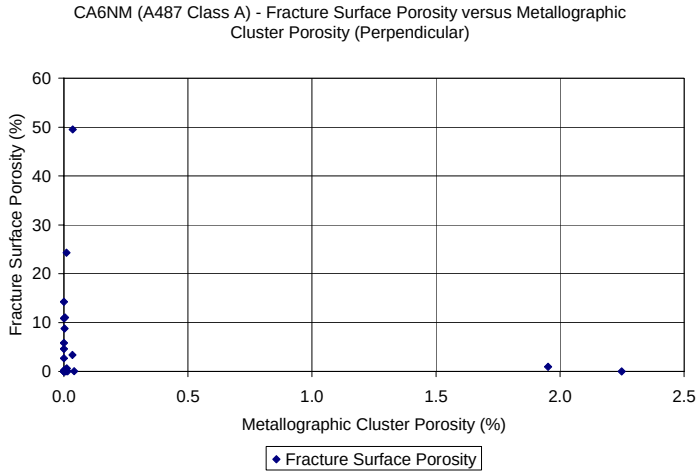

Figure 92. Relationship between fracture surface porosity and metallographic porosity in CA6NM.

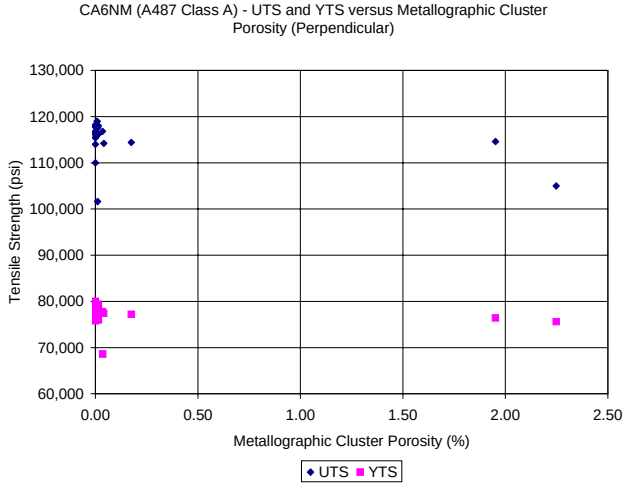

Figure 93. Relationship between tensile strength and metallographic porosity in CA6NM.

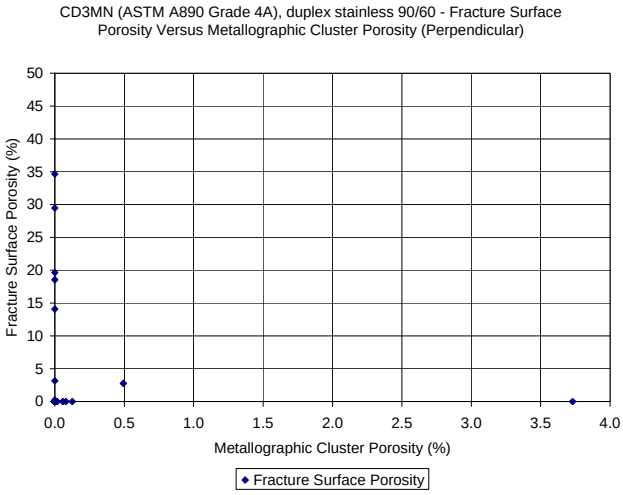

Figure 94. Relationship between fracture surface porosity and metallographic porosity in CD3MN.

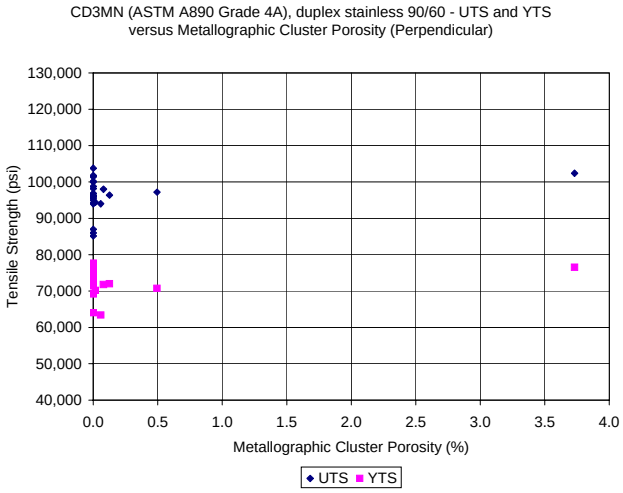

Figure 95. Relationship between tensile strength and metallographic porosity in CD3MN.

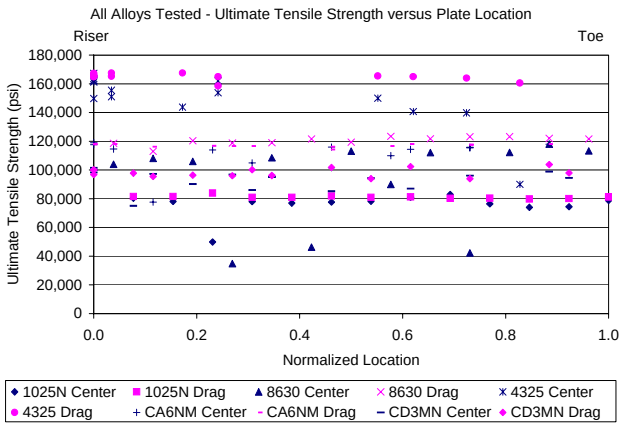

Figure 96. Relationship between UTS of all alloys and specimen location.

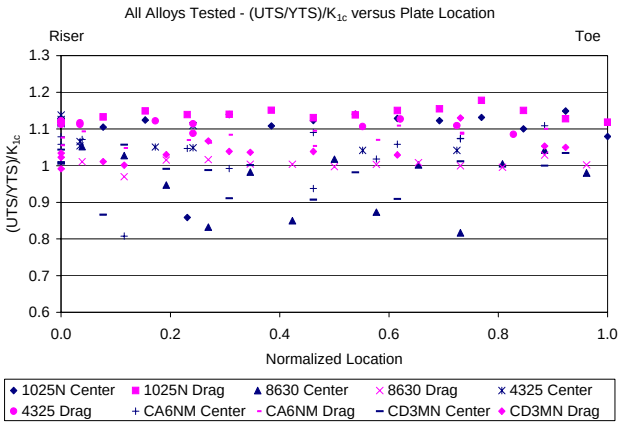

Figure 97. Relationship between normalized tensile strength of all alloys and specimen location.

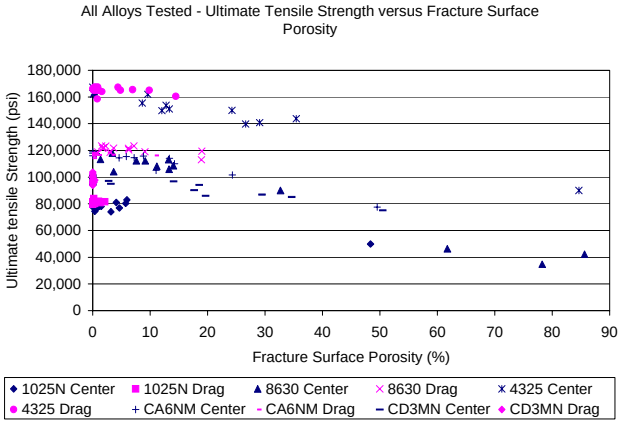

Figure 98. Relationship between UTS of all alloys and fracture surface porosity.

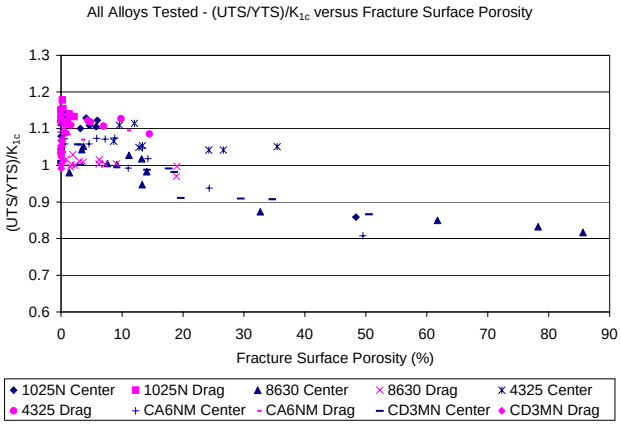

Figure 99. Relationship between normalized tensile strength of all alloys and fracture surface porosity.

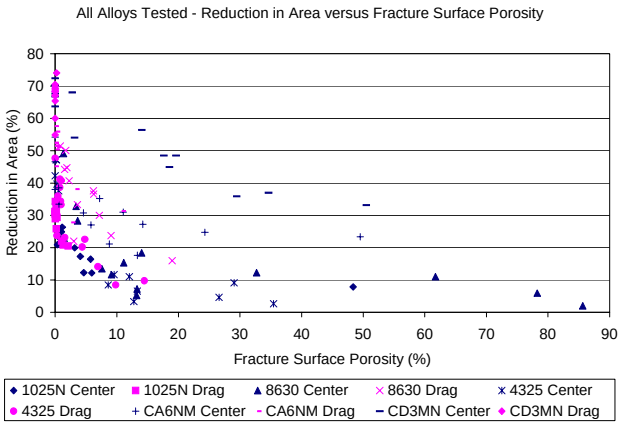

Figure 100. Relationship between reduction in area of all alloys and fracture surface porosity.

5. ACKNOWLEDGMENTS

We wish to thank the Department of Energy, the Cast Metals Coalition and the Steel Founders' Society of America for financially supporting this project. We wish to express grateful acknowledgment and deep appreciation to the many companies and individuals who participated in the project by providing advice, descriptions of particular difficulties, defects, and guidance. We also wish to thank the Falk Corporation, Harrison Steel, Southwest Steel, and Wollaston Steel for producing and heat treating the test plates used in the experiments.

A special word of thanks goes to Malcolm Blair at SFSA for guidance throughout the project. We also wish to express our appreciation to the Department of Energy for technical assistance and partial funding of the project. Special thanks go to Bob Trimberger, Ehr Ping Huangfu and Dibyajyoti Aichbhaumik. Matching funds from DOE were provided under Cooperative Agreement DE-FC36-02ID14229 with Amendments. Matching funds were also provided to the Iowa State University.

6. REFERENCES

1. Chvorinov, N., *Giesserei*, 27, 1940, pp 177-186.
2. Pellini, W.S., "Factors which Determine Riser Adequacy and Feeding Range", *AFS Transactions*, Vol. 61, 1953, pp61-80.
3. Flinn, R.A., P.J. Guichelarr, and M.J. Weins, "Riser Size and Placement for Copper Alloy Castings", *AFS Transactions*, Vol. 73, 1965, pp 355-361.
4. Caine, J.B., "A Theoretical Approach to the Problem of Dimensioning Risers", *AFS Transactions*, Vol. 56, 1948, pp 492-501.
5. Niyama, E., T. Uchida, M. Morikawa, and S. Saito, "A Method of Shrinkage Prediction and Its Application to Steel Casting Practice", *AFS Int. Cast Metals Res. Jnl*., 7, 1982, pp 52-63.
6. Murthy, K., M. Seshadri, and A. Ramachadrian, "End Chills Thermal Behavior and Effect on Casting Soundness", *AFS Transactions*, Vol. 73, 1965, pp.502-508.
7. Uram, S.Z., M.C. Flemings, and H.F.Taylor, "High Strength Cast Steel Structure and Microporosity Effect on Mechanical Properties", *AFS Transactions*, Vol. 68, 1960, pp 347-360.
8. Larson, H.R., H.W. Lloyd, and F.B. Herlihy, "Comparison of X-Ray Quality and Tensile Properties in Cast High Strength Steel", *AFS Transactions*, Vol. 67, 1959, pp 676-384.

USE OF THIS REPORT AND INFORMATION CONTAINED THEREIN

Limitation of Liability

The faculty and staff of UAB associated with this project have used their professional experience and best professional efforts in performing this work. However, UAB not represent, warrant or guarantee that its research results, or product produced therefrom, are merchantable or satisfactory for any particular purpose, and there are no warranties, express or implied, to such effect. Acceptance, reliance on, or use of such results shall be at the sole risk of Sponsor. In connection with this work, UAB shall in no event be responsible or liable in contract or in tort for any special, indirect, incidental or consequential damages, such as, but not limited to, loss of product, profits or revenues, damage or loss from operation or nonoperation of plant, or claims of customers of Sponsor.

Report No.: 527992-2005 Project Final Report

To: Department of Energy; The Steel Founders' Society of America.

Date: September 9, 2005